arXiv:1403.2276v1 [astro-ph.EP] 10 Mar 2014

New insights on Titan's interior from its obliquity

Benoît Noyelles

NAmur Center for CompleX SYStems (naXys) – University of Namur – Rempart de la Vierge 8 – B-5000 Namur – Belgium

benoit.noyelles@unamur.be

and

Francis Nimmo

Department of Earth and Planetary Sciences – University of California at Santa Cruz – 1156 High Street – Santa Cruz, California 95064 – USA

fnimmo@es.ucsc.edu

Received _____; accepted _____

ABSTRACT

We constructed a 6-degrees of freedom rotational model of Titan as a 3-layer body consisting of a rigid core, a fluid global ocean, and a floating ice shell. The ice shell exhibits partially-compensated lateral thickness variations in order to simultaneously match the observed degree-two gravity and shape coefficients. The rotational dynamics are affected by the gravitational torque of Saturn, the gravitational coupling between the inner core and the shell, and the pressure coupling at the fluid-solid boundaries. Between 10 and 13% of our model Titans have an obliquity (due to a resonance with the 29.5-year periodic annual forcing) that is consistent with the observed value.

The shells of the successful models have a mean thickness of 130 to 140 km, and an ocean of ≈250 km thickness. Our simulations of the obliquity evolution show that the *Cassini* obliquity measurement is an instantaneous one, and does not represent a mean value. Future measurements of the time derivative of the obliquity would help to refine the interior models. We expect in particular a variation of roughly 7 arcmin over the duration of the *Cassini* mission.

Subject headings: Celestial Mechanics – Resonances, spin-orbit – Rotational dynamics – Titan, interior

1. Introduction

The *Cassini* spacecraft, in orbit around Saturn since July 2004, has allowed huge progress on modelling of the internal structure and the rotational dynamics of Titan. An internal ocean is consistent with the measurements of the tidal Love number $k_2 \approx 0.6$ (Iess et al. 2012) and was theoretically predicted by Lunine & Stevenson (1987), this prediction being supported by several following studies, e.g. (Grasset & Sotin 1996; Grasset et al. 2000; Tobie et al. 2005; Fortes et al. 2007). A comparison between the shape of Titan (Zebker et al. 2009) (Tab.1) and its gravity field (Iess et al. 2010) (Tab.2) suggests either variations in the thickness of a floating ice shell (Nimmo & Bills 2010; Hemingway et al. 2013) or lateral variations in the shell's density (Choukroun & Sotin 2012).

Table 1: The shape of Titan, from (Zebker et al. 2009).

Parameter	Value
Subplanetary equatorial radius a	2575.15 ± 0.02 km
Along orbit equatorial radius b	2574.78 ± 0.06 km
Polar radius c	2574.47 ± 0.06 km
Mean radius R	2574.73 ± 0.09 km

EDITOR: PLACE TABLE 1 HERE.

EDITOR: PLACE TABLE 2 HERE.

Cassini observed Titan's rotation as well. The most recent measurements suggest the expected synchronous rotation (Meriggiola & Iess 2012) and a pretty high obliquity of $\approx 0.3^\circ$ at the mean date March 11^{th} 2007, already detected by (Stiles et al. 2008). If we

assume that the rotation of Titan has reached its most probable dynamical equilibrium state, i.e. Cassini State 1, then this obliquity is not consistent with a rigid Titan (Noyelles et al. 2008; Bills & Nimmo 2008, 2011). However, the presence of an internal ocean can lead to a resonant process raising the obliquity of Titan (Baland et al. 2011), making the high obliquity a possible signature of a global subsurface ocean.

In this paper, we simulate the rotation of Titan, considering both the internal structure and all the dynamical degrees of freedom. Our Titan is a 3-layer body composed of a rigid inner core, a global ocean and rigid shell with a variable thickness. For each of the 2 rigid layers, we simulate at the same time the longitudinal motion, the orientation of the angular momentum, and of the figure polar axis. The dynamics of these 2 layers will be affected by the gravitational pull of Saturn, the pressure coupling at the interface with the ocean and the gravitational coupling between them. The pressure coupling is modelled after Baland et al. (2011) and the gravitational coupling after Szeto & Xu (1997). In calculating the torques, we take into account variations in the thickness of the ice shell (Nimmo & Bills 2010) consistent with the gravity and topography constraints. We then identify interior structures for which the predicted rotation state is consistent with the observations, before simulating the expected behavior of the obliquity of Titan.

Our model confirms the conclusion of Baland et al. (2011) that the unexpectedly high obliquity of Titan could be due to a resonance with the periodic annual forcing. We go further, however, in showing that the obliquity is predicted to be time-variable (Fig 9): a prediction which analysis of *Cassini* radar observations (Bills et al. 2013) should be able to test.

2. The equations of the problem

The approach that we follow below is a generalization of the scheme adopted by Baland et al. (2011). There are two important innovations in our approach. First, we consider the three-dimensional orientation of the shell and of the core, so that we can simultaneously treat both obliquity (Bills & Nimmo 2011; Baland et al. 2011) and also longitudinal librations (Van Hoolst et al. 2013; Richard et al. 2014), as well as determining the magnitude of the usually neglected polar motion. Second, we explicitly take into account the rigidity and spatial variations in thickness of the ice shell, which are indicated by Titan's topography and gravity (Nimmo & Bills 2010; Hemingway et al. 2013) and which affect the resulting torques.

Although our model is quite complicated, it does neglect some potentially significant effects. Most notably, we do not consider the effects of either atmospheric torques or torques due to flow in the subsurface ocean. The low viscosity of water argues against the latter being important, but in some cases tidal forcing can lead to strong flows (Noir et al. 2009; Cebron et al. 2012). We defer consideration of this topic to future work. As discussed below, we also neglect the potential effect of restoring torques due to elastic deformation of the ice shell (Goldreich & Mitchell 2010; Richard et al. 2014).

2.1. Parameterization of the problem

We simulate the orientation of both the rigid inner core and the rigid shell (or crust). For that, we need 2 sets of Euler angles, respectively $(h^c, \epsilon^c, \theta^c)$ for the core and $(h^s, \epsilon^s, \theta^s)$ for the shell to represent the orientation of the principal axes of inertia of the considered layer in an inertial reference frame (Fig.1).

EDITOR: PLACE FIGURE 1 HERE.

These Euler angles present a virtual singularity. If the quantity ϵ is null, then the angles h and θ are not uniquely defined, but their sum is. In practice, it appears that when ϵ is small enough, then numerical uncertainties can erronously suggest an erratic behavior. We by-passed this problem by using the following cartesian-like coordinates:

$$\begin{aligned} \xi^{s,c} &= \epsilon^{s,c} \sin h^{s,c}, \\ \eta^{s,c} &= \epsilon^{s,c} \cos h^{s,c}, \\ p^{s,c} &= h^{s,c} + \theta^{s,c}. \end{aligned}$$

When ϵ is null, then η and ξ are both null and the system does not present any singularity.

We also need to represent the angular momentum $\vec{G}$ of each of these rigid layers. For that we use as variables the components of the associated rotation vector $\vec{\omega}$; this yields $\vec{G^s} = A^s\omega_1^s\vec{f_1^s} + B^s\omega_2^s\vec{f_2^s} + C^s\omega_3^s\vec{f_3^s}$ for the shell and $\vec{G^c} = A^c\omega_1^c\vec{f_1^c} + B^c\omega_2^c\vec{f_2^c} + C^c\omega_3^s\vec{f_3^c}$ for the core. A, B and C are the principal moments of inertia of the layer under consideration; we have for the core:

$$A^c = \iiint_{core} \rho_c(x,y,z)\left(y^2+z^2\right) dxdydz, \quad (1)$$

$$B^c = \iiint_{core} \rho_c(x,y,z)\left(x^2+z^2\right) dxdydz, \quad (2)$$

$$C^c = \iiint_{core} \rho_c(x,y,z)\left(x^2+y^2\right) dxdydz, \quad (3)$$

and similar formulae for the shell. $\rho_c(x,y,z)$ is the density of the core, (x,y,z) being the classical writings for the cartesian coordinates, in the reference frame of the principal axes of inertia $(\vec{f_1^c}, \vec{f_2^c}, \vec{f_3^c})$.

2.2. Kinematic equations controlling the Euler angles

To determine the relations linking the Euler angles of a layer to the components of the angular momentum, we have to keep in mind the geometry of the problem (Fig.1). As explained for instance in (Fowles & Cassiday 1999), the rotation vector $\vec{\omega} = \omega_1 \vec{f_1} + \omega_2 \vec{f_2} + \omega_3 \vec{f_3}$ represents 3 successive rotations:

1. a rotation around the z-axis (here $\vec{e_3}$) of an angle h,
2. then a rotation around the new, but not final, x-axis of angle ϵ,
3. and finally a rotation around the final z-axis, i.e. $\vec{f_3}$, of an angle θ.

This reads mathematically:

$$\begin{pmatrix} \omega_1 \\ \omega_2 \\ \omega_3 \end{pmatrix} = \begin{pmatrix} 0 \\ 0 \\ \dot{\theta} \end{pmatrix} + R_3(-\theta) \begin{pmatrix} \dot{\epsilon} \\ 0 \\ 0 \end{pmatrix} + R_3(-\theta) R_1(-\epsilon) \begin{pmatrix} 0 \\ 0 \\ \dot{h} \end{pmatrix}, \tag{4}$$

with

$$R_3(\phi) = \begin{pmatrix} \cos\phi & -\sin\phi & 0 \\ \sin\phi & \cos\phi & 0 \\ 0 & 0 & 1 \end{pmatrix} \tag{5}$$

and

$$R_1(\phi) = \begin{pmatrix} 1 & 0 & 0 \\ 0 & \cos\phi & -\sin\phi \\ 0 & \sin\phi & \cos\phi \end{pmatrix}. \tag{6}$$

This yields

$$\omega_1 = \dot{\epsilon}\cos\theta + \dot{h}\sin\epsilon\sin\theta, \tag{7}$$

$$\omega_2 = -\dot{\epsilon}\sin\theta + \dot{h}\sin\epsilon\cos\theta, \tag{8}$$

$$\omega_3 = \dot{\theta} + \dot{h}\cos\epsilon, \tag{9}$$

and

$$\dot{h} = \frac{\omega_1\sin\theta + \omega_2\cos\theta}{\sin\epsilon}, \tag{10}$$

$$\dot{\epsilon} = \omega_1\cos\theta - \omega_2\sin\theta, \tag{11}$$

$$\dot{\theta} = \omega_3 - \frac{\omega_1\sin\theta + \omega_2\cos\theta}{\tan\epsilon}. \tag{12}$$

The equations (10) and (12) illustrate the virtual singularity we mentioned above. These formulae are the same as the ones present in (Black et al. 1995; Harbison et al. 2011) but are given with a different sign in numerous other studies, e.g. (Williams et al. 2001), probably because of a different sign convention. We now get straightforwardly:

$$\dot{\xi} = (\omega_1\cos\theta - \omega_2\sin\theta)\sin h + \frac{\epsilon}{\sin\epsilon}(\omega_1\sin\theta + \omega_2\cos\theta)\cos h, \tag{13}$$

$$\dot{\eta} = (\omega_1\cos\theta - \omega_2\sin\theta)\cos h - \frac{\epsilon}{\sin\epsilon}(\omega_1\sin\theta + \omega_2\cos\theta)\sin h, \tag{14}$$

$$\dot{p} = \omega_3 + (\omega_1\sin\theta + \omega_2\cos\theta)\tan\frac{\epsilon}{2}. \tag{15}$$

The virtual singularity has nearly disappeared. The only numerical problem that could remain is due to $\epsilon/\sin\epsilon$ in the Eq.(13) and (14), so we replace it by its Taylor expansion $1 + \epsilon^2/6 + 7\epsilon^4/360$ for $\|\epsilon\| < 10^{-8}$.

As shown in (Baland et al. 2011), the dynamical equations reduce to

$$\frac{d\overrightarrow{G^c}}{dt} = \overrightarrow{\Gamma^c_{\hbar}} + \overrightarrow{\Gamma^c_o} + \overrightarrow{\Gamma^c_{sh}}, \quad (16)$$

$$\frac{d\overrightarrow{G^s}}{dt} = \overrightarrow{\Gamma^s_{\hbar}} + \overrightarrow{\Gamma^s_o} + \overrightarrow{\Gamma^s_{co}}, \quad (17)$$

the relevant torques being:

- $\overrightarrow{\Gamma^c_{\hbar}}$: gravitational torque of Saturn on the core,
- $\overrightarrow{\Gamma^c_o}$: pressure coupling of the ocean at the core-ocean boundary,
- $\overrightarrow{\Gamma^c_{sh}}$: gravitational torque of the shell on the core,
- $\overrightarrow{\Gamma^s_{\hbar}}$: gravitational torque of Saturn on the shell,
- $\overrightarrow{\Gamma^s_o}$: pressure coupling of the ocean at the shell-ocean boundary,
- $\overrightarrow{\Gamma^s_{co}}$: gravitational torque of the core on the shell.

Baland et al. (2011) have shown that the sum of the torques acting on the ocean is null if the fluid is in hydrostatic equilibrium.

Since we work in the non-inertial reference frames of the principal axes of inertia of the core $(\vec{f}^c_1, \vec{f}^c_2, \vec{f}^c_3)$, and of the shell $(\vec{f}^s_1, \vec{f}^s_2, \vec{f}^s_3)$, we must add $-\vec{\omega^c} \times \vec{G^c}$ in Eq.(16) and $-\vec{\omega^s} \times \vec{G^s}$ in Eq.(17).

We now detail the torques affecting the rotation.

2.3. The gravitational pull of Saturn

For a rigid triaxial body whose principal moments of inertia are $A < B < C$, the gravitational torque of a perturber is classically given by:

$$\vec{\Gamma} = \frac{3\mathcal{G}M_{\text{ħ}}}{\|\overrightarrow{r_{\text{ħ}}}\|^5}\left((C-B)y_{\text{ħ}}z_{\text{ħ}}\vec{f_1} + (A-C)x_{\text{ħ}}z_{\text{ħ}}\vec{f_2} + (B-A)x_{\text{ħ}}y_{\text{ħ}}\vec{f_3}\right), \tag{18}$$

where $\mathcal{G}$ is the gravitational constant, $M_{\text{ħ}}$ the mass of the perturber, and the vector $\overrightarrow{r_{\text{ħ}}} = x_{\text{ħ}}\vec{f_1} + y_{\text{ħ}}\vec{f_2} + z_{\text{ħ}}\vec{f_3}$ locates the perturber from the center of mass of the triaxial body. In our case, this is the Titan-Saturn vector. A derivation of this torque is proposed in (Murray & Dermott 2000), inspired from (MacMillan 1936; Ramsey 1937, 1940).

We here treat the inner core and the shell as 2 independent triaxial rigid bodies, and we have:

$$\overrightarrow{\Gamma^c_{\text{ħ}}} = \frac{3\mathcal{G}M_{\text{ħ}}}{\|\overrightarrow{r^c_{\text{ħ}}}\|^5}\left((C^c-B^c)y^c_{\text{ħ}}z^c_{\text{ħ}}\overrightarrow{f^c_1} + (A^c-C^c)x^c_{\text{ħ}}z^c_{\text{ħ}}\overrightarrow{f^c_2} + (B^c-A^c)x^c_{\text{ħ}}y^c_{\text{ħ}}\overrightarrow{f^c_3}\right), \tag{19}$$

$$\overrightarrow{\Gamma^s_{\text{ħ}}} = \frac{3\mathcal{G}M_{\text{ħ}}}{\|\overrightarrow{r^s_{\text{ħ}}}\|^5}\left((C^s-B^s)y^s_{\text{ħ}}z^s_{\text{ħ}}\overrightarrow{f^s_1} + (A^s-C^s)x^s_{\text{ħ}}z^s_{\text{ħ}}\overrightarrow{f^s_2} + (B^s-A^s)x^s_{\text{ħ}}y^s_{\text{ħ}}\overrightarrow{f^s_3}\right). \tag{20}$$

We use the TASS1.6 ephemerides (Vienne & Duriez 1995) to express the Titan-Saturn vector $\vec{r_{\text{ħ}}}$. These ephemerides are presented under a quasiperiodic form, in which every sinusoidal contribution due to any perturber like Saturn's oblateness or the Solar attraction is explicitly expressed. They are given in the inertial reference frame defined by the equatorial plane of Saturn at J2000 and the node of this plane with the ecliptic at the same date. As an example, in this reference frame, the quantities related to the inclination of Titan I_6 and its ascending Ω_6 (Titan is denoted as *S-6 Titan*) are

$$\sin\left(\frac{I_6(t)}{2}\right)\exp\left(\imath\Omega_6(t)\right) = \gamma_0\exp\left(\imath\Omega_0\right) + \sum_{i=1}^{4}\gamma_i\exp\left(\imath\Omega_i(t)\right), \tag{21}$$

the quantities γ_i and Ω_i being given in the Tab.3.

Similar tables exist for the mean motion, the mean longitude, and the quantity relevant to the eccentricity e_6 and the longitude of the pericenter ϖ_6, i.e. $z_6 = e_6\exp\left(\imath\varpi_6\right)$.

The TASS1.6 ephemerides are probably not the most accurate we could get, but they have the huge advantage of being presented in a quasiperiodic form giving explicitly the different contributions affecting Titan's orbit. From the periods of the sinusoidal quantities indexed from 1 to 4 in the Eq.(21) and the Tab.3, we can say that $i = 1$ corresponds to the motion of the ascending node induced by the oblateness of Saturn, $i = 2$ is a perturbation by Iapetus, and $i = 3, 4$ correspond to the Solar orbital perturbation, the orbital period of Saturn around the Sun being 29.46 years. It is impossible to have such a decomposition with the JPL HORIZON ephemerides since they are given over a too short timespan ($\approx$ 400 years) with respect to the relevant periods. This is why we choose to use TASS1.6, Baland et al. (2011) having made the same choice.

The choice of the reference frame is not straightforward. To get an obliquity having a straightforward physical meaning, it is often advisable to use the Laplace Plane, that minimizes the variations of the inclination. Unfortunately, there are in the literature several inconsistent definitions of the Laplace Plane, since there are several ways to minimize the variations of the inclination (over which time interval should we minimize? how do we measure the variations of the inclination?...). Noyelles (2009) suggests using the constant term in the quasiperiodic decomposition of the inclination to define the inertial reference frame. This is a kind of averaging of the orbital plane, that is very close to the Laplace Plane. In particular, this choice avoids a problem of apparent erratic behavior of the rotation pole that could happen for a satellite orbiting far off its parent planet, when the rings' plane is chosen as the reference plane. The reason is that these satellites usually have a significantly inclined orbit because of the Solar perturbation.

This is why our reference frame is obtained from the reference frame of the ephemerides after 2 rotations: a R_3 rotation of 184.578°, and a R_1 rotation of 0.642°, these numbers being derived from the line $i = 0$ in the Tab.3. A very easy way to implement these

rotations is just to drop $\gamma_0 \exp(\imath\Omega_0)$ from Eq.(21).

After a straightforward calculation we get from TASS1.6 the Titan-Saturn vector $\vec{r_0}$ in the inertial reference frame that we just defined, and then the vector $\overrightarrow{r_{\hbar}^{c,s}}$ after 3 rotations of the Euler angles:

$$\overrightarrow{r_{\hbar}^{c}} = R_3(-\theta^c)R_1(-\epsilon^c)R_3(-h^c)\vec{r_0}, \quad (22)$$

$$\overrightarrow{r_{\hbar}^{s}} = R_3(-\theta^s)R_1(-\epsilon^s)R_3(-h^s)\vec{r_0}. \quad (23)$$

At this time we can simulate the rotation of the inner core and the rigid shell as two independent rigid bodies. We successfully checked our code in comparing with the results given by the numerical code based on an Hamiltonian formalism that we used in several previous studies (Noyelles et al. 2008; Noyelles 2009, 2010; Noyelles et al. 2011).

2.4. The gravitational coupling between the inner core and the shell

This subsection is based on Szeto & Xu (1997), in which the gravitational coupling between the shell and the core of the Earth is estimated. This gravitational coupling is due to the misalignment of the principal axes of inertia of these 2 layers. We now need to be more specific as to their structure:

- The inner core is a triaxial ellipsoid with a constant density ρ_c, its radii being denoted $c_c < b_c < a_c$. Its surface is the core-ocean boundary.
- The shell (or crust) has a constant density ρ_s as well. Its shape can be described by two concentric and coaxial triaxial ellipsoids. The radii of the outer one are denoted $c < b < a$, they correspond to the observed shape of Titan (Zebker et al. 2009), while

the inner one is aligned with the outer one, its radii are denoted $c_o < b_o < a_o$. This inner edge of the crust is the shell-ocean boundary. It is important to define a_o,b_o,c_o as well as a,b and c to allow for the possibility of lateral shell thickness variations, which Nimmo & Bills (2010) argued are likely to exist.

Following Szeto & Xu (1997), the gravitational torque acting on the inner core due to the shell reads:

$$\overrightarrow{\Gamma_{sh}^{c}} = \iiint_{core} \rho_c \vec{r} \times \vec{\nabla}\Phi dV, \tag{24}$$

where $\vec{r}$ points in this subsection to the position of a mass element of the core, and Φ is the potential of the shell given by (Szeto & Xu 1997):

$$\Phi = \alpha + \beta r^2 P_2(\cos\psi) + \gamma r^2 P_2^2(\cos\psi)\cos 2\phi + \mathcal{O}(f_{1,2}^2, \kappa_{1,2}^2), \tag{25}$$

where

- α is a constant that does not affect the result,
- $\beta = \frac{4\pi}{15}\mathcal{G}\rho_s(\kappa_2 - \kappa_1 - 2(f_2 - f_1))$,
- $\gamma = \frac{2\pi}{15}\mathcal{G}\rho_s(\kappa_2 - \kappa_1)$,
- $f_1 = (a_o - c_o)/a_o$ is the polar flattening of the shell-ocean boundary,
- $f_2 = (a - c)/a$ is the polar flattening of the surface of Titan,
- $\kappa_1 = (a_o - b_o)/a_o$ is the equatorial ellipticy of the shell-ocean boundary,
- $\kappa_2 = (a - b)/a$ is the equatorial ellipticity of the surface of Titan,
- $P_2(x) = (3x^2 - 1)/2$ is a Legendre polynomial,

- $P_2^2(x) = 3(1-x^2)$ is a Legendre associated function,
- ψ and ϕ are respectively the colatitude and the east longitude of the mass element involved, in the reference frame of the principal axes of inertia of the shell $\left(\overrightarrow{f_1^s}, \overrightarrow{f_2^s}, \overrightarrow{f_3^s}\right)$.

After some algebra (see App.A) we get

$$\overrightarrow{\Gamma_{sh}^c} = 3\beta \begin{bmatrix} n_2 n_3 (C^c - B^c) \overrightarrow{f_1^c} \\ -n_1 n_3 (C^c - A^c) \overrightarrow{f_2^c} \\ n_1 n_2 (B^c - A^c) \overrightarrow{f_3^c} \end{bmatrix} + 6\gamma \begin{bmatrix} (l_2 l_3 - m_2 m_3)(C^c - B^c) \overrightarrow{f_1^c} \\ -(l_1 l_3 - m_1 m_3)(C^c - A^c) \overrightarrow{f_2^c} \\ (l_1 l_2 - m_1 m_2)(B^c - A^c) \overrightarrow{f_3^c} \end{bmatrix}, \quad (26)$$

where l_i, m_i and n_i $(i = 1, 2, 3)$ are the elements of the transition matrix between the coordinates in the reference frame of the shell (X, Y, Z) and the ones in the reference frame of the core (x, y, z), i.e.

$$\begin{pmatrix} X \\ Y \\ Z \end{pmatrix} = \begin{pmatrix} l_1 & l_2 & l_3 \\ m_1 & m_2 & m_3 \\ n_1 & n_2 & n_3 \end{pmatrix} \begin{pmatrix} x \\ y \\ z \end{pmatrix}. \quad (27)$$

An analogous calculation gives us the torque of the inner core acting on the shell:

$$\overrightarrow{\Gamma_{co}^s} = -3\beta \begin{bmatrix} n_2 n_3 (C^c - B^c) \overrightarrow{f_1^s} \\ -n_1 n_3 (C^s - A^c) \overrightarrow{f_2^s} \\ n_1 n_2 (B^c - A^c) \overrightarrow{f_3^s} \end{bmatrix} - 6\gamma \begin{bmatrix} (l_2 l_3 - m_2 m_3)(C^c - B^c) \overrightarrow{f_1^s} \\ -(l_1 l_3 - m_1 m_3)(C^c - A^c) \overrightarrow{f_2^s} \\ (l_1 l_2 - m_1 m_2)(B^c - A^c) \overrightarrow{f_3^s} \end{bmatrix}. \quad (28)$$

2.5. Influence of the ocean

Baland et al. (2011) have shown that if the ocean is in hydrostatic equilibrium, then the pressure torque can be expressed as additional terms in the gravitational torques acting

on the two rigid layers. We can split the ocean into two parts: a top and a bottom one, their boundary being spherical. The resulting pressure torque integrated over a spherical boundary is null, so the radius of this sphere has no influence on the results (an outcome we verified numerically).

We call A_t^o, B_t^o, C_t^o, A_b^o, B_b^o and C_b^o the principal moments of inertia, respectively of the top ocean in the reference frame of the shell $(\vec{f_1^s}, \vec{f_2^s}, \vec{f_3^s})$ and of the bottom ocean in the reference frame of the core $(\vec{f_1^c}, \vec{f_2^c}, \vec{f_3^c})$. Instead of writing the contribution of the ocean as independent torques $\vec{\Gamma_o^c}$ and $\vec{\Gamma_o^s}$, it is more appropriate to alter the other torques as $\overrightarrow{\Gamma_{\mathfrak{h}}^{c,o}}$, $\overrightarrow{\Gamma_{\mathfrak{h}}^{s,o}}$, $\overrightarrow{\Gamma_{sh}^{c,o}}$, and $\overrightarrow{\Gamma_{co}^{s,o}}$. And we have:

$$\overrightarrow{\Gamma_{\mathfrak{h}}^{c,o}} = \frac{3\mathcal{G}M_{\mathfrak{h}}}{\|\vec{r_{\mathfrak{h}}^c}\|^5}((C^c - B^c + C_b^o - B_b^o)y_{\mathfrak{h}}^c z_{\mathfrak{h}}^c \vec{f_1^c} + (A^c - C^c + A_b^o - C_b^o)x_{\mathfrak{h}}^c z_{\mathfrak{h}}^c \vec{f_2^c} + (B^c - A^c + B_b^o - A_b^o)x_{\mathfrak{h}}^c y_{\mathfrak{h}}^c \vec{f_3^c}), \tag{29}$$

$$\overrightarrow{\Gamma_{\mathfrak{h}}^{s,o}} = \frac{3\mathcal{G}M_{\mathfrak{h}}}{\|\vec{r_{\mathfrak{h}}^s}\|^5}((C^s - B^s + C_t^o - B_t^o)y_{\mathfrak{h}}^s z_{\mathfrak{h}}^s \vec{f_1^s} + (A^s - C^s + A_t^o - C_t^o)x_{\mathfrak{h}}^s z_{\mathfrak{h}}^s \vec{f_2^s} + (B^s - A^s + B_t^o - A_t^o)x_{\mathfrak{h}}^s y_{\mathfrak{h}}^s \vec{f_3^s}), \tag{30}$$

$$\overrightarrow{\Gamma_{sh}^{c,o}} = \begin{bmatrix} (3\beta^o n_2 n_3 + 6\gamma^o(l_2 l_3 - m_2 m_3))\,(C^c - B^c + C_b^o - B_b^o)\vec{f_1^c} \\ -(3\beta^o n_1 n_3 + 6\gamma^o(l_1 l_3 - m_1 m_3))\,(C^c - A^c + C_b^o - A_b^o)\vec{f_2^c} \\ (3\beta^o n_1 n_2 + 6\gamma^o(l_1 l_2 - m_1 m_2))\,(B^c - A^c + B_b^o - A_b^o)\vec{f_3^c} \end{bmatrix}, \tag{31}$$

and

$$\overrightarrow{\Gamma_{co}^{s,o}} = \begin{bmatrix} -(3\beta^o n_2 n_3 + 6\gamma^o(l_2 l_3 - m_2 m_3))\,(C^c - B^c + C_b^o - B_b^o)\vec{f_1^s} \\ (3\beta^o n_1 n_3 + 6\gamma^o(l_1 l_3 - m_1 m_3))\,(C^c - A^c + C_b^o - A_b^o)\vec{f_2^s} \\ -(3\beta^o n_1 n_2 + 6\gamma^o(l_1 l_2 - m_1 m_2))\,(B^c - A^c + B_b^o - A_b^o)\vec{f_3^s} \end{bmatrix}, \tag{32}$$

with

$$\beta^o = \frac{4\pi}{15}\mathcal{G}\left(\rho_s\left(\kappa_2 - \kappa_1 - 2(f_2 - f_1)\right) + \rho_o\left(\kappa_1 - 2f_1\right)\right), \quad (33)$$

$$\gamma^o = \frac{2\pi}{15}\mathcal{G}\left(\rho_s(\kappa_2 - \kappa_1) + \rho_o\kappa_1\right), \quad (34)$$

ρ_o being the constant density of the ocean.

We have now the whole equations of the problem, consisting of 12 variables ξ^c, η^c, p^c, ω_1^c, ω_2^c, ω_3^c, ξ^s, η^s, p^s, ω_1^s, ω_2^s, ω_3^s, the first 6 describing the orientation of the core, and the last 6 the orientation of the shell. The components of the rotation vector $\vec{\omega}$ in the reference frame of the principal axes of inertia of the considered layer are obtained from the angular momentun $\vec{G}$ and division by the appropriate moment of inertia.

As a summary, we here gather these equations. We have:

$$\frac{d\xi^c}{dt} = (\omega_1^c \cos\theta^c - \omega_2^c \sin\theta^c) \sin h^c + \frac{\epsilon^c}{\sin\epsilon^c} (\omega_1^c \sin\theta^c + \omega_2^c \cos\theta^c) \cos h^c, \tag{35}$$

$$\frac{d\eta^c}{dt} = (\omega_1^c \cos\theta^c - \omega_2^c \sin\theta^c) \cos h^c - \frac{\epsilon^c}{\sin\epsilon^c} (\omega_1^c \sin\theta^c + \omega_2^c \cos\theta^c) \sin h^c, \tag{36}$$

$$\frac{dp^c}{dt} = \omega_3^c + (\omega_1^c \sin\theta^c + \omega_2^c \cos\theta^c) \tan\frac{\epsilon^c}{2}, \tag{37}$$

$$\begin{aligned}\frac{d\omega_1^c}{dt} &= (3\beta^o n_2 n_3 + 6\,(l_2 l_3 - m_2 m_3))\,\frac{C^c - B^c + C_b^o - B_b^o}{A^c} \\ &+ 3\frac{\mathcal{G}M_\natural}{||\overrightarrow{r_\natural^c}||^5}\frac{C^c - B^c + C_b^o - B_b^o}{A^c} y_\natural^c z_\natural^c - \frac{\left(\vec{\omega^c} \times \vec{G^c}\right) \cdot \overrightarrow{f_1^c}}{A^c},\end{aligned} \tag{38}$$

$$\begin{aligned}\frac{d\omega_2^c}{dt} &= -(3\beta^o n_1 n_3 + 6\,(l_1 l_3 - m_1 m_3))\,\frac{C^c - A^c + C_b^o - A_b^o}{B^c} \\ &+ 3\frac{\mathcal{G}M_\natural}{||\overrightarrow{r_\natural^c}||^5}\frac{A^c - C^c + A_b^o - C_b^o}{B^c} x_\natural^c z_\natural^c - \frac{\left(\vec{\omega^c} \times \vec{G^c}\right) \cdot \overrightarrow{f_2^c}}{B^c},\end{aligned} \tag{39}$$

$$\begin{aligned}\frac{d\omega_3^c}{dt} &= (3\beta^o n_1 n_2 + 6\,(l_1 l_2 - m_1 m_2))\,\frac{B^c - A^c + B_b^o - A_b^o}{C^c} \\ &+ 3\frac{\mathcal{G}M_\natural}{||\overrightarrow{r_\natural^c}||^5}\frac{B^c - A^c + B_b^o - A_b^o}{C^c} x_\natural^c y_\natural^c - \frac{\left(\vec{\omega^c} \times \vec{G^c}\right) \cdot \overrightarrow{f_3^c}}{C^c}\end{aligned} \tag{40}$$

for the core, and

$$\frac{d\xi^s}{dt} = (\omega_1^s \cos\theta^s - \omega_2^s \sin\theta^s) \sin h^s + \frac{\epsilon^s}{\sin\epsilon^s} (\omega_1^s \sin\theta^s + \omega_2^s \cos\theta^s) \cos h^s, \tag{41}$$

$$\frac{d\eta^s}{dt} = (\omega_1^s \cos\theta^s - \omega_2^s \sin\theta^s) \cos h^s - \frac{\epsilon^s}{\sin\epsilon^s} (\omega_1^s \sin\theta^s + \omega_2^s \cos\theta^s) \sin h^s, \tag{42}$$

$$\frac{dp^s}{dt} = \omega_3^s + (\omega_1^s \sin\theta^s + \omega_2^s \cos\theta^s) \tan\frac{\epsilon^s}{2}, \tag{43}$$

$$\begin{aligned}\frac{d\omega_1^s}{dt} &= -\left(3\beta^o n_2 n_3 + 6\left(l_2 l_3 - m_2 m_3\right)\right) \frac{C^c - B^c + C_b^o - B_b^o}{A^s} \\ &+ 3\frac{\mathcal{G}M_\hbar}{||\overrightarrow{r_\hbar^s}||^5} \frac{C^s - B^s + C_t^o - B_t^o}{A^s} y_\hbar^s z_\hbar^s - \frac{\left(\vec{\omega^s} \times \vec{G^s}\right) \cdot \overrightarrow{f_1^s}}{A^s},\end{aligned} \tag{44}$$

$$\begin{aligned}\frac{d\omega_2^s}{dt} &= \left(3\beta^o n_1 n_3 + 6\left(l_1 l_3 - m_1 m_3\right)\right) \frac{C^c - A^c + C_b^o - A_b^o}{B^s} \\ &+ 3\frac{\mathcal{G}M_\hbar}{||\overrightarrow{r_\hbar^s}||^5} \frac{A^s - C^s + A_t^o - C_t^o}{B^s} x_\hbar^s z_\hbar^s - \frac{\left(\vec{\omega^s} \times \vec{G^s}\right) \cdot \overrightarrow{f_2^s}}{B^s},\end{aligned} \tag{45}$$

$$\begin{aligned}\frac{d\omega_3^s}{dt} &= -\left(3\beta^o n_1 n_2 + 6\left(l_1 l_2 - m_1 m_2\right)\right) \frac{B^c - A^c + B_b^o - A_b^o}{C^s} \\ &+ 3\frac{\mathcal{G}M_\hbar}{||\overrightarrow{r_\hbar^s}||^5} \frac{B^s - A^s + B_t^o - A_t^o}{C^s} x_\hbar^s y_\hbar^s - \frac{\left(\vec{\omega^s} \times \vec{G^s}\right) \cdot \overrightarrow{f_3^s}}{C^s}\end{aligned} \tag{46}$$

for the shell.

Table 2: The 2 solutions for the gravity field of Titan (Iess et al. 2010). SOL1 is a single multiarc solution obtained from 4 flybys of *Cassini* dedicated to the determination of the gravity field, while SOL2 is a more general approach, in which all available radiometric tracking and optical navigation imaging data from the Pioneer and Voyager Saturn encounters and astronomical observations of Saturn and its satellites are considered. The uncertainties correspond to 1σ. The global solution SOL2 could be consistent with the hydrostatic equilibrium ($J_2/C_{22} \approx 10/3$), but the shape is not (Zebker et al. 2009). In our study of a triaxial Titan, the only coefficients we use are $\mathcal{G}M_6$, J_2 and C_{22}.

	SOL1	SOL2
$\mathcal{G}M_6$	–	8978.1394 $km^3.s^{-2}$
J_2	$(3.1808 \pm 0.0404) \times 10^{-5}$	$(3.3462 \pm 0.0632) \times 10^{-5}$
C_{21}	$(3.38 \pm 3.50) \times 10^{-7}$	$(4.8 \pm 11.5) \times 10^{-8}$
S_{21}	$(-3.52 \pm 4.38) \times 10^{-7}$	$(6.20 \pm 4.96) \times 10^{-7}$
C_{22}	$(9.983 \pm 0.039) \times 10^{-6}$	$(1.0022 \pm 0.0071) \times 10^{-5}$
S_{22}	$(2.17 \pm 0.41) \times 10^{-7}$	$(2.56 \pm 0.72) \times 10^{-7}$
J_3	$(-1.879 \pm 1.019) \times 10^{-6}$	$(-7.4 \pm 105.1) \times 10^{-8}$
C_{31}	$(1.058 \pm 0.260) \times 10^{-6}$	$(1.805 \pm 0.297) \times 10^{-6}$
S_{31}	$(5.09 \pm 2.02) \times 10^{-7}$	$(2.83 \pm 3.54) \times 10^{-7}$
C_{32}	$(3.64 \pm 1.13) \times 10^{-7}$	$(1.36 \pm 1.58) \times 10^{-7}$
S_{32}	$(3.47 \pm 0.80) \times 10^{-7}$	$(1.59 \pm 1.05) \times 10^{-7}$
C_{33}	$(-1.99 \pm 0.09) \times 10^{-7}$	$(-1.85 \pm 0.12) \times 10^{-7}$
S_{33}	$(-1.71 \pm 0.15) \times 10^{-7}$	$(-1.49 \pm 0.16) \times 10^{-7}$
J_2/C_{22}	3.186 ± 0.042	3.339 ± 0.067

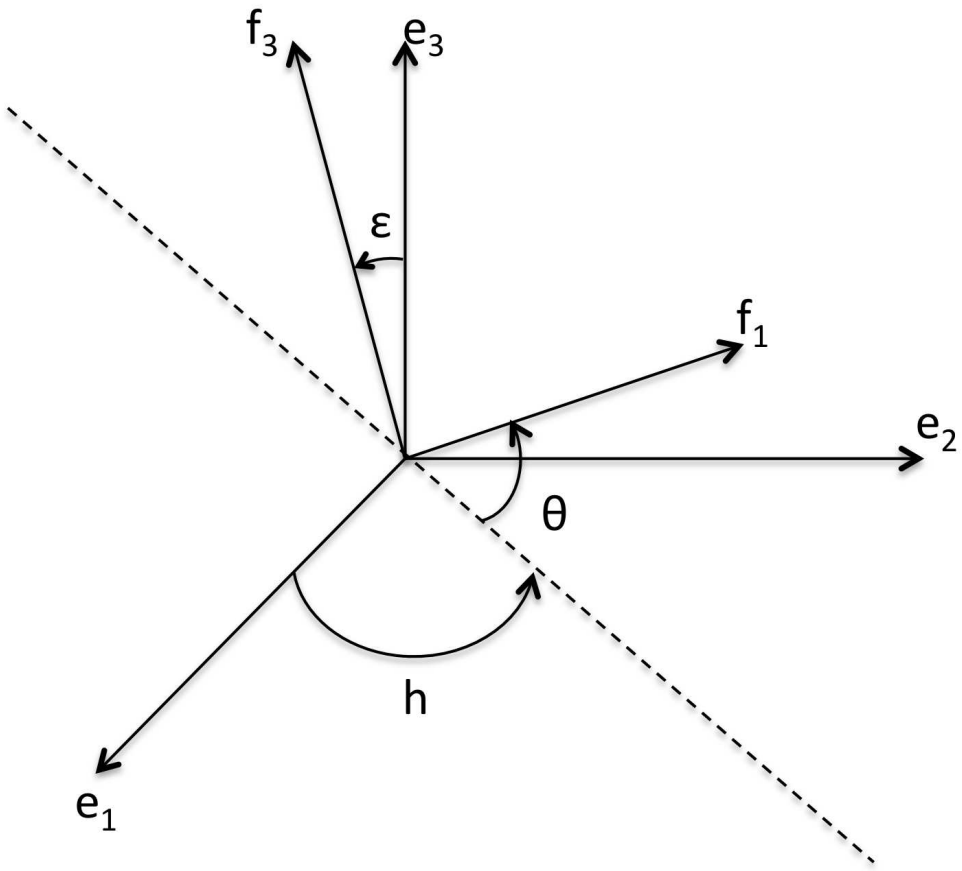

Fig. 1.— Euler angles (h, ϵ, θ) giving the orientation of the principal axes of inertia $(\vec{f_1}, \vec{f_2}, \vec{f_3})$ of a rigid layer (inner core or shell) with respect to the inertial reference frame $(\vec{e_1}, \vec{e_2}, \vec{e_3})$. These quantities should be written with a superscript c or s, i.e. either h^c or h^s whether they are related to the inner core or to the shell. The dashed line is the intersection between the inertial reference plane $(\vec{e_1}, \vec{e_2})$ and the equatorial plane of the core or shell $(\vec{f_1}, \vec{f_2})$.

Table 3: Relevant quantities for the orbital inclination and ascending node of Titan, reproduced from (Vienne & Duriez 1995). These numbers are to be used into the Eq.21. The time origin is here J2000.

i	Amplitude γ_i	Phase $\Omega_i(t=0)$	$d\Omega_i/dt$ (rad/y)	Period (years)
0	5.6024×10^{-3}	184.578°	0	–
1	2.7899×10^{-3}	-14.731°	-8.93124×10^{-3}	703.51
2	1.312×10^{-4}	-73.192°	-1.92554×10^{-3}	3263.07
3	1.126×10^{-4}	117.445°	0.42659824	14.73
4	1.92×10^{-5}	47.498°	−0.21329912	29.46

3. A numerical solution

A numerical solution of the equations (35) to (46) is here appropriate since we want to include complete ephemerides and 6 dynamical degrees of freedom.

3.1. Numerical integration of the equations

The numerical integrations are performed with the Adams-Bashforth-Moulton 10th order predictor corrector integrator (see e.g. (Hairer et al. 2003)), with a tolerance of 10^{-14} and a step size of 0.2 day. This corresponds to $\approx 1/80$ of the orbital period of Titan.

The rotation of Titan is expected to be at a dynamical equilibrium. Such equilibriums are known as Cassini States (Cassini 1693; Colombo 1966; Peale 1969) for rigid bodies. The expected state for the natural satellites of the giant planets is Cassini State 1 since it is the most stable. In our case of a 3-layer Titan, we initially assume an analogous state in which the inner core and the crust are close to the location of Cassini State 1 if they were only interacting with Saturn. This state corresponds to a synchronous rotation, a small obliquity and a small polar motion. As a consequence, the angular momentum of the shell and the core should approximate $\overrightarrow{G^s} \approx n_6 C^s \overrightarrow{f_3^s}$ and $\overrightarrow{G^c} \approx n_6 C^c \overrightarrow{f_3^c}$ where n_6 is the mean motion, or orbital frequency, of Titan, and the spin angles of the core p^c and of the shell p^s should be always close to the orbital mean longitude of Titan λ_6.

Because of the effects that are neglected in the theory of the Cassini States, especially the couplings between the different layers and the perturbations considered in the orbital motion of Titan, it is very difficult to derive analytically the optimal initial conditions for the Euler angles and the rotation vector. In practice, our initial conditions are usually close enough to the optimum state that oscillations round the equilibrium result, these free oscillations having an arbitrary amplitude due to the choice of the initial conditions, and a

proper frequency whose value depends on the parameters of the system, here the interior of Titan. These free oscillations pollute the analysis of the solutions in acting as a noise, for this reason we wish their amplitude to be as small as possible. For that, we refine numerically the initial conditions thanks to an iterative algorithm based on the frequency analysis.

The basic idea is that since the orbital motion of Titan can be given under a quasiperiodic form, and that the rotation of Titan is not expected to be chaotic, then this rotation can be expressed under a quasiperiodic form as well. A complex variable $x(t)$ of the problem that does not diverge can read as a sum of a converging trigonometric series like

$$x(t) = \sum_{n=0}^{\infty} A_n \exp\left(\imath \nu_n t\right), \tag{47}$$

where A_n are constant complex amplitudes, and ν_n constant frequencies, with

$$x(t) \approx \sum_{n=0}^{N} A_n^{\bullet} \exp\left(\imath \nu_n^{\bullet} t\right), \tag{48}$$

the bullet meaning that the coefficients have been numerically determined. A detailed description of the algorithm is given in Appendix B. In the case of a real variable, Eq.48 becomes

$$x(t) \approx \sum_{n=0}^{N} A_n^{\bullet} \cos\left(\nu_n^{\bullet} t + \phi_n^{\bullet}\right), \tag{49}$$

or

$$x(t) \approx \sum_{n=0}^{N} A_n^{\bullet} \sin\left(\nu_n^{\bullet} t + \phi_n^{\bullet}\right), \tag{50}$$

where the amplitudes are now real, and the $\phi_n^\bullet$ are real phases, previously included in the complex amplitudes in Eq.48.

The frequency analysis algorithm we use is based on NAFF (see (Laskar 1993) for the method, and (Laskar 2005) for the convergence proofs), with a refinement suggested by (Champenois 1998) consisting in iterating the process to improve the accuracy of the determination. The frequencies ν_n have 2 origins: they might be either forcing frequencies, present in the orbital motion of Titan, or free frequencies, due to the departure from the exact equilibrium. The amplitude associated with the latter should be as small as possible. To get the appropriate initial conditions we use an iterative algorithm (Noyelles et al. 2014), consisting in:

1. A first numerical integration of the equations of the system, with initial conditions conveniently chosen,
2. Frequency analysis of the solution and identification of the contributions depending on the free modes,
3. Evaluation of the free modes at the origin time of the numerical simulation, and removal from the initial conditions,

then the process is iterated until convergence. This algorithm has already been successfully applied in problem of rotational dynamics (Dufey et al. 2009; Noyelles 2009; Robutel et al. 2011), in dynamics of exoplanetary systems (Couetdic et al. 2010), and in the analysis of ground-track resonances around Vesta (Delsate 2011).

We know of at least 3 alternative methods to reduce the amplitude of the free librations:

- Bois & Rambaux (2007) propose to fit the mean initial conditions in order to locate the spin-orbit system at its center of libration,

- Peale et al. (2007) add a damping in the equations that reduces the amplitude of the free librations. The damping must be slow enough, i.e. adiabatic, to not alter significantly the location of the equilibrium,

- Yseboodt & Margot (2006), in the framework of a numerical integration of the spin and of the orbit of Mercury, start from a simple Sun-Mercury system in which the equilibrium is very easy to determine analytically, and slowly switch on the planetary perturbations in order to create an adiabatic devitation of the equilibrium without creation of any free libration. In our case, this would require us to simultaneously integrate the orbit of Titan, rather than use the existing ephemerides.

All of these methods, including ours, give accurate results when appropriately used.

In this study, we simulated the rotation of thousands of model Titans (see Sec.4) and did not refine the initial conditions for all of them. In practice, we did it for just a few of them, and got initial conditions that we considered to be good enough for the remainder.

3.2. Outputs

Our set of variables describes all the dynamical degrees of freedom of the core and the shell, so we are able to express any observable of the rotation. Our outputs are, for these two rigid layers:

- the longitudinal librations,

- the obliquity,

- and the polar motion.

The longitudinal librations of the shell are usually considered as the most significant output since they can reveal a global fluid layer (Van Hoolst et al. 2008). There are at least two ways to define them: the tidal librations and the physical librations. The tidal librations $\psi^{s,c}$ represent the longitudinal misalignment between the directions of the long axis of the layer under consideration (the shell or the core) and the Saturn-Titan direction. The physical significance of these librations is that they control the amount of tidal stress and heating arising. They are given by

$$\psi^s = \vec{t} \cdot \vec{f_1^s}, \tag{51}$$

$$\psi^c = \vec{t} \cdot \vec{f_1^c}, \tag{52}$$

where $\vec{t}$ is the unit vector tangent to the trajectory of Titan around Saturn:

$$\vec{t} = \frac{\vec{n} \times \vec{x}}{||\vec{n} \times \vec{x}||}, \tag{53}$$

and $\vec{n}$ the unit vector normal to the orbit:

$$\vec{n} = \frac{\vec{x} \times \vec{v}}{||\vec{x} \times \vec{v}||}, \tag{54}$$

$\vec{x}$ and $\vec{v}$ being respectively the position vector of Titan, and $\vec{v}$ its velocity.

The physical librations $\gamma^{s,c}$ are the librations about the exact synchronous rotation. We derived them from the variable $p^{s,c} - n_6 t$, this is a very good approximation if the angles $\epsilon^{s,c}$ are small, i.e. if the two angles h^s and θ^s constituting p^s, respectively h^c and θ^c for p^c, are nearly coplanar. In practice, the angles ϵ^s and ϵ^c are always smaller than 1 degree. They also correspond, up to the first order in eccentricity, to the librations of the long axis of the considered layer with the direction of the empty focus of the orbit of Titan.

The difference between the tidal and the physical librations are known as optical librations, their amplitude is twice the eccentricity e_6 and is just a signature of the orbital motion, not of the interior of the body. In practice, the tidal librations are dominated by the optical librations. This is why the physical librations are usually preferred to the tidal ones, their amplitude is roughly proportional to the difference of the moments of inertia (B-A) for rigid bodies.

In the case of Titan, longitudinal librations have not so far been detected, although analysis of *Cassini* radar images may ultimately make this possible (Bills et al. 2013, e.g.).

The obliquity of the shell K^s (respectively of the core K^c) is defined as the angle between the normale to the orbit $\vec{n}$ and the angular momentum of the shell $\overrightarrow{G^s}$ (respectively of the core $\overrightarrow{G^c}$). Since an obliquity belongs to the range [0°-180°], we can define it with its cosine and we have:

$$K^s = \arccos\left(\frac{\vec{n}\cdot\overrightarrow{G^s}}{||\overrightarrow{G^s}||}\right), \quad (55)$$

$$K^c = \arccos\left(\frac{\vec{n}\cdot\overrightarrow{G^c}}{||\overrightarrow{G^c}||}\right). \quad (56)$$

Cassini measured an obliquity of the shell of $0.31° \pm 0.05°$, i.e. (18.6 ± 3) arcmin at the mean date March 11^{th}, 2007 (Meriggiola & Iess 2012).

The polar motion is a priori expected to be very small and is often neglected. We did include polar motion in our numerical simulations for completeness, and in case resonances or nonlinearities in the rotational dynamics resulted in large polar motion, as suggested for a rigid Titan by (Noyelles 2008), and for a Titan with a thin shell and a strong atmospheric torque in (Tokano et al. 2011). However, in every simulation polar motion remained very small.

4. Possible interiors of Titan

The goal of this section is to build realistic models for Titan, that will give us the interior parameters we need in our numerical code, i.e. the density and the 3 outer radii of the inner core, the ocean and the shell. The three external radii of the shell are known thanks to *Cassini* observations (Zebker et al. 2009). To build our Titans, our algorithm consists of 3 steps:

1. Elaboration of hydrostatic Titans. The choice of this starting point comes from the observations that the gravity field of Titan is not far from a hydrostatic one,
2. Modification of the hydrostatic state by including shell thickness variations, imposed at either the surface (top loading) or at the ocean-shell boundary (bottom loading),
3. Comparison with the gravity field. Only model Titans for which the gravity field is consistent with the observations are retained.

For each model Titan, we set the densities of the shell ρ_s and of the ocean ρ_o, and the mean thicknesses of the shell d_s and of the ocean d_o. The size and density of the core can then be deduced, the mean density of Titan being $\rho_6 = 1881\ kg/m^3$ (Iess et al. 2010). Note that in our approach the core can potentially include high-pressure phases of ice; the importance of the core is that it represents the base of the decoupling ocean. The range of internal parameters we consider are:

- d_s between 50 and 200 km,
- d_o between 50 and $400 - d_s$ km,
- ρ_s between 900 and 950 kg/m^3,

- ρ_o between 950 and 1200 kg/m^3.

The range of possible densities for the ocean comes from Fortes (2012). The limit of the depth of the core-ocean interface comes from the condition of existence of a liquid ocean with respect to the temperature and the pressure, see the phase diagram of water ice (Sotin et al. 2010) and of an ammonia-water ocean (Sohl et al. 2003). Even for a warm ocean (270 K), the pressure at the base of the ocean should be smaller than 0.6 GPa, which corresponds to a depth of about 450 km. Since ammonia is likely to be present, 270 K is likely an overestimate, so we consider that 400 km is a reasonable limit for the depth of the core-ocean boundary.

We here build initially hydrostatic Titans, following a method described in Van Hoolst et al. (2008). A body in hydrostatic equilibrium has a shape corresponding to a balance between its own gravity, its rotation and the tidal deformation. Its surface is an equipotential, and the 2 boundaries between the different layers are equipotential as well. We consider that the mean radius $R = 2574.73$ km and the along-orbit equatorial radius $b = 2574.78$ km are known. We then obtain from the Radau equation (see e.g. (Jeffreys 1952)):

$$h_2 = \frac{5}{1+\left(\frac{5}{2}-\frac{15}{4}\frac{C}{M_6R^2}\right)^2}, \quad (57)$$

$$q = \frac{n_6^2R^3}{\mathcal{G}M_6}, \quad (58)$$

$$\tilde{c} = b - \frac{h_2}{2}qR, \quad (59)$$

$$\tilde{a} = b + \frac{3}{2}qh_2R, \quad (60)$$

where h_2 is the second-order fluid Love number related to the radial displacement. $\tilde{a}$ and $\tilde{c}$ are radii of this hydrostatic Titan, they should be very close to a and c.

$q = 3.95428 \times 10^{-5}$ quantifies the relative influence between the rotation of Titan and its own gravity. $C = C^s + C^o + C^c$ is the polar moment of inertia of the whole Titan. In the Eq.(57), $C/(M_6R^2)$ is in fact used as an approximation of $I/(M_6R^2) = (A+B+C)/(3M_6R^2) = C/(M_6R^2) - 2J_2/3$. At this stage, the shape of Titan is unknown, so we neglect J_2 and we estimate C from the mean radius R and the mean thicknesses of the shell d_s and the ocean d_o, i.e.

$$C \approx \frac{8\pi}{15}\left((\rho_c - \rho_o)\left(R - d_s - d_o\right)^5 + (\rho_o - \rho_s)\left(R - d_s\right)^5 + \rho_s R^5\right). \tag{61}$$

The Radau equation comes from the solution of the Clairaut equation that gives the flattening $\alpha = (a+b-2c)/(a+b)$ of the equipotential surface at any radius r:

$$\frac{d^2\alpha}{dr^2} + \frac{6}{r}\frac{\rho}{\bar{\rho}} - \frac{6}{r^2}\left(1 - \frac{\rho}{\bar{\rho}}\right)\alpha = 0, \tag{62}$$

$$\frac{d\alpha}{dr}(R) = \frac{1}{R}\left[\frac{25}{4}q - 2\alpha(R)\right], \tag{63}$$

$$\alpha(R) = \frac{\tilde{a} + b - 2\tilde{c}}{\tilde{a} + b}. \tag{64}$$

The initial condition (63) is not the classical one given in the Clairaut theory where 25/4 should be replaced by 5/2, because it considers the deformations due to the rotation, and the tides. Moreover, we have $\beta = 6\alpha/5 = (\tilde{a} - b)/\tilde{a}$ at any radial distance r. This can be easily seen at $r = R$. From the classical relation $(\tilde{a} - \tilde{c}) = 4(b - \tilde{c})$ for hydrostatic synchronous bodies, we have straightforwardly $\alpha = 5/3 \times (\tilde{a} - b)/(\tilde{a} + b) \approx 5\beta/6$. A more rigorous proof, valid at any radial distance r, can be found in (Van Hoolst et al. 2008). We then get the three radii of the core-ocean and of the ocean-shell boundaries.

These hydrostatic Titans do not correspond to the real one. In particular, the two model external radii $\tilde{a}$ and $\tilde{c}$ are not consistent with the observations. We solve this problem

by introducing a topographic anomaly at the surface h_t:

$$h_t(\psi,\phi) = h_{t1}Y_{20}(\psi) + h_{t2}Y_{22}(\psi,\phi) \tag{65}$$

where Y_{20} and Y_{22} are the classical second-degree spherical harmonics defined by:

$$Y_{lm}(\psi,\phi) = \sqrt{(2-\delta_{0m})\,(2l+1)\frac{(l-m)!}{(l+m)!}}P_{lm}(\cos\psi))\cos m\phi \tag{66}$$

for $m > 0$. P_{l0} are the Legendre polynomials and P_{lm} the associated Legendre functions for $m \neq 0$ already defined in Subs.2.4. Eq.(65) becomes

$$h_t(\psi,\phi) = \frac{\sqrt{5}}{2}h_{t1}\left(3\cos^2\psi - 1\right) + 3\sqrt{\frac{5}{12}}h_{t2}\sin^2\psi\cos 2\phi. \tag{67}$$

We now set $\Delta a = a - \tilde{a}$ and $\Delta c = c - \tilde{c}$ the two radial anomalies corresponding respectively to $(\psi = k\pi)$ and $(\psi = k\pi, \phi = 2k'\pi)$, where k and k' are integers. We have:

$$\Delta c = \sqrt{5}h_{t1}, \tag{68}$$

$$\Delta a = -\frac{\sqrt{5}}{2}h_{t1} + 3\sqrt{\frac{5}{12}}h_{t2}, \tag{69}$$

from which we deduce h_{t1} and h_{t2}.

It follows from the definition of the spherical harmonics that the radius b is altered as well. For this reason, we need to iterate the process in correcting the initial value of b, so that the surface of our model Titan has the correct radii a, b and c at the end.

As suggested by Nimmo & Bills (2010); Hemingway et al. (2013), the topographic anomaly could be caused by variations of the thickness of the ice shell and partial or complete isostatic compensation (see e.g.(Watts 2001)). So, there should be a corresponding

bottom anomaly h_b altering the shape of the ocean-shell boundary following the same spherical harmonics, i.e.

$$h_b(\psi, \phi) = h_{b1} Y_{20}(\psi) + h_{b2} Y_{22}(\psi, \phi). \tag{70}$$

It is useful to distinguish between a load applied at the surface of Titan (top loading) and a load applied at the ocean-shell boundary (bottom loading). Top loading results in bottom topography h_b given by:

$$h_b = f h_t \left(\frac{R}{R - d_s} \right)^2 \frac{\rho_s}{\rho_o - \rho_s}, \tag{71}$$

while bottom loading gives the following surface topography:

$$h_t = f h_b \left(\frac{R - d_s}{R} \right)^2 \frac{\rho_o - \rho_s}{\rho_s}. \tag{72}$$

Here $f \in [0; 1]$ is the compensation factor. $f = 0$ means that there is no compensation, the shell is perfectly rigid, and loading does not cause any deformation of the shell. Contrariwise, $f = 1$ means full compensation, so that the top- and bottom-loading cases are indistinguishable.

Once these model Titans have been computed, their second-degree gravity fields are calculated and only the ones consistent with the gravity solutions SOL1 or SOL2 are kept. Because the degree-3 gravity, not modelled here but treated in detail by Hemingway et al. (2013), is more consistent with bottom loading than with top loading, we focus more on the former. The only acceptable solutions we get with top loading lie between the 2σ and 3σ limits for SOL2. They are not displayed here since they cannot explain the observations (see Sect.5).

Fig. 2 shows some properties of our model Titans. We can see in particular that the gravity field constrains the degree-two compensation factor f to a range roughly 0.75-0.95, very similar to the results obtained by Hemingway et al. (2013). In other words, the bottom load is mostly but not entirely compensated. The differences between the maximum and minimum thickness of the shell are shown in Fig.3. They can reach 38 km when the densities of the core and of the shell are very close, while they do not exceed 60 meters when Titan is in hydrostatic equilibrium.

We note that our approach assumes that all the non-hydrostatic effects are contained within the ice shell, i.e. the core is hydrostatic. This assumption can be justified based on the strong observed correlation at degree-3 between the shell surface topography and the gravity (Hemingway et al. 2013); a low-rigidity (and likely hydrostatic) core is also indicated by the large tidal response of Titan (Iess et al. 2012).

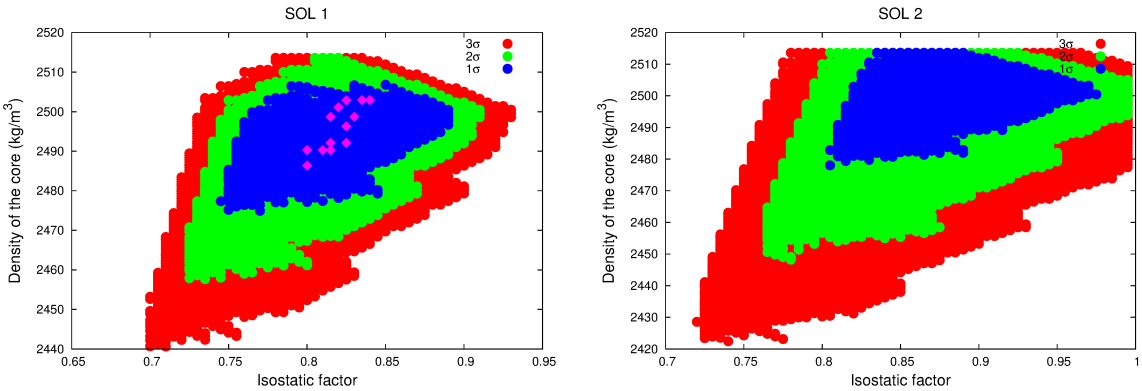

Fig. 2.— Properties of our model Titans, complying with the 2 possible gravity fields SOL1 (multi-arc) and SOL2 (global), at 1σ (blue), 2σ (green) and 3σ (red). These 2 plots have been obtained assuming bottom loading. We can see in particular that SOL1 suggests a compensation factor between 75 and 88%, while SOL2 suggests between 80 and 96% at 1σ. The left panel also shows 13 model Titans that will be used later to simulate the behavior of the obliquity.

EDITOR: PLACE FIGURE 2 HERE.

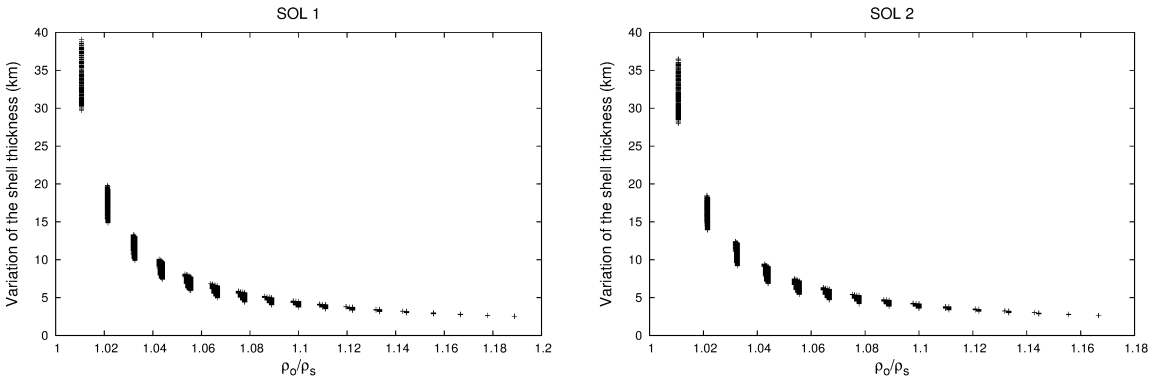

Fig. 3.— Thickness variations of the shell of our Titans. Here only the 1σ solutions are displayed, the results being not significantly different when extended to 3σ.

EDITOR: PLACE FIGURE 3 HERE.

5. Results

We here present the results of the numerical simulations of the rotational dynamics of Titan for 71,046 interior models, 20,526 consistent with SOL1 (2,237 of them at 1σ) and 50,500 with SOL2 (2,681 of them at 1σ).

5.1. Longitudinal librations

We here show the amplitude of the physical longitudinal librations $\gamma^{s,c}$ at the orbital frequency. This amplitude is denoted g^s for the shell (Fig.4) and g^c for the core. These amplitudes have been obtained numerically, but they are in very good agreement with the ones given by the analytical formulae (see Appendix C).

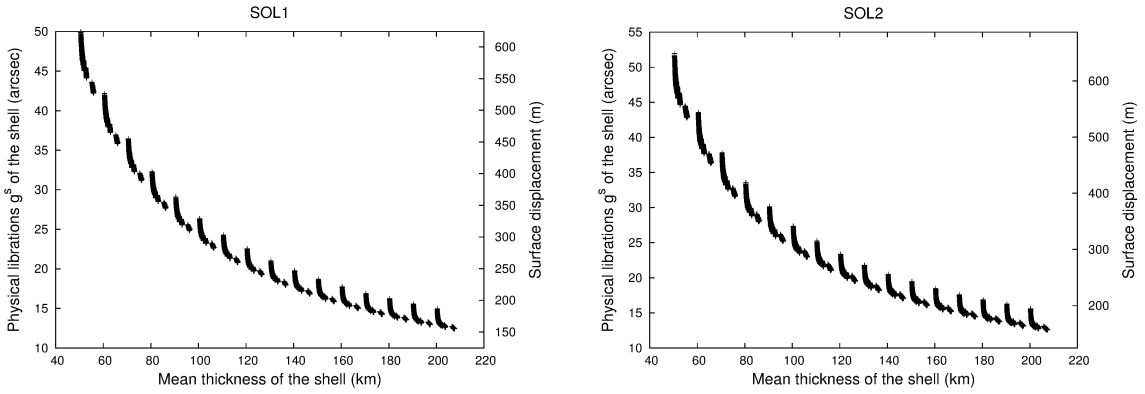
SOL1
Physical librations g^s of the shell (arcsec)
Surface displacement (m)
Mean thickness of the shell (km)
SOL2
Physical librations g^s of the shell (arcsec)
Surface displacement (m)
Mean thickness of the shell (km)

Fig. 4.— Longitudinal librations of the shell.

EDITOR: PLACE FIGURE 4 HERE.

We get an amplitude of libration g^s that can reach 600 meters for a thin shell. One important caveat here is that we are neglecting the rigidity of the ice shell, which tends to oppose librational motion (Goldreich & Mitchell 2010), and which in the case of Titan is thought to be large (Hemingway et al. 2013). When elasticity is considered, the

amplitude of libration could be 10 times smaller (Van Hoolst et al. 2013; Richard et al. 2014); (Jara-Orué & Vermeersen 2014) have found a similar result for Europa.

Van Hoolst et al. (2009) have shown that when the atmospheric torque was considered, then the main librations were the semi-annual, with a period of 14.29 years. That study used the atmospheric torque published by (Tokano & Neubauer 2005). (Richard et al. 2014) have shown that using the global climate model of (Lebonnois et al. 2012) gives a smaller amplitude. We here do not consider the atmospheric torque and do not detect a significant 14.29-y periodic oscillation.

For the core, we predict a much smaller amplitude of libration, between 2.1 and 2.6 arcmin. The two periods of free librations associated are respectively between 200 and 400 days, and between 2.5 and 2.7 years. These periods do not allow any resonance with forcing frequencies, and so the libration amplitudes are not raised.

5.2. A resonant obliquity of the shell

The obliquity of the shell is the only rotational quantity that has been measured, beside the spin rate. Its value of $0.31^\circ \pm 0.05^\circ$ (Meriggiola & Iess 2012) is surprisingly high (see Sec.1). To the best of our knowledge, the only satisfying explanation present in the literature (Baland et al. 2011) is a resonance between the free librations of the obliquity and a forced oscillation due to either the Solar gravitational perturbation of 29.46 years or the regression of Titan's ascending node around Saturn, the period associated being 703.51 years. A resonance is usually a strong phenomenon, that is efficient over a limited range of parameters. An issue is the probability that Titan be affected by such a resonance.

EDITOR: PLACE FIGURE 5 HERE.

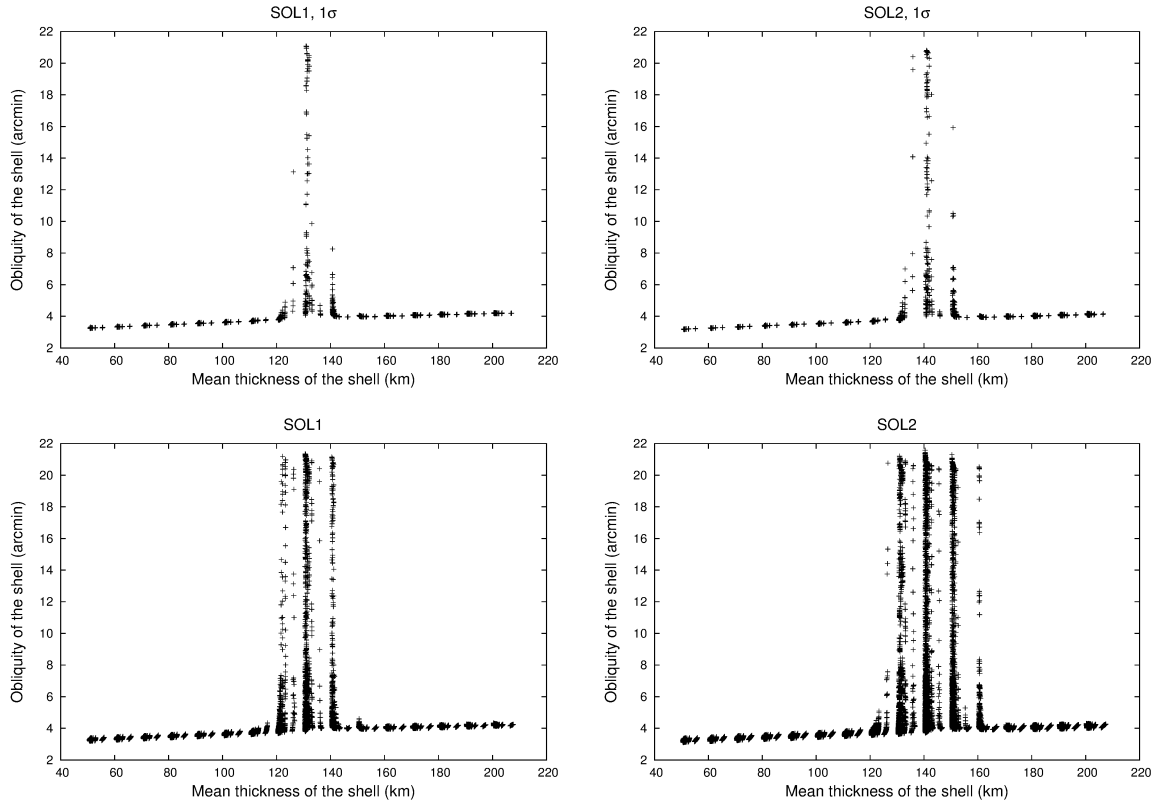

Fig. 5.— Influence of the thickness of the shell on its obliquity.

EDITOR: PLACE FIGURE 6 HERE.

Figs.5 and 6 show the mean obliquity of the shell with respect to the mean thickness of the shell and the ocean. We plot here the results for model Titans with a gravity field within the $1-\sigma$ limit of the measured one, and within the $3-\sigma$ limit. We can see two regimes for the obliquity. Most of the solutions lie on a nearly constant line, indicating an obliquity between 3 and 4.2 arcmin. This is the obliquity given by the classical theory of a rigid body in a secular regime. These numbers are too small with respect to the measured one, i.e. ≈ 18 arcmin. However, another regime with much higher obliquities can be seen, for thicknesses of the shell and of the ocean of ≈ 130 and ≈ 270 km for SOL1, and ≈ 140 and ≈ 260 km for SOL2. Since a resonance is suspected, we determine the periods of the

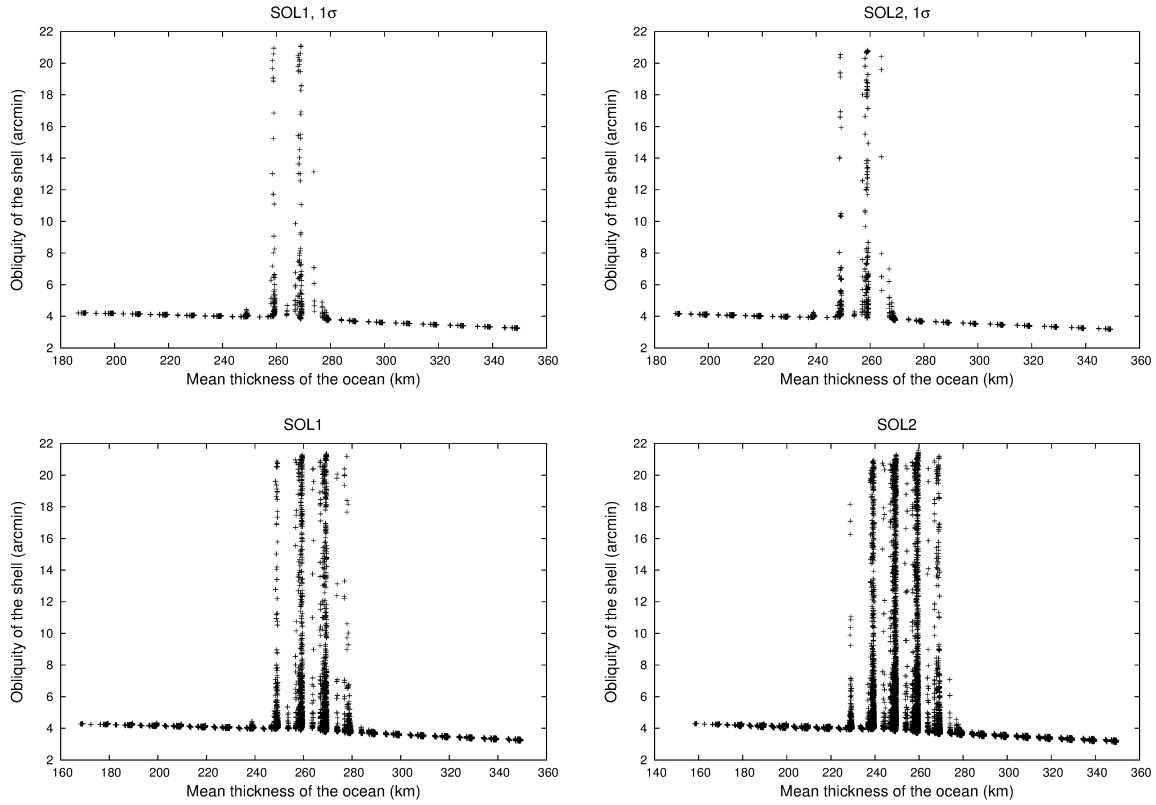

Fig. 6.— Influence of the thickness of the ocean on the obliquity of the shell.

free oscillations associated with the obliquity.

In adapting a result by Baland et al. (2011), the frequencies of these free librations σ_3 and σ_4 are:

$$\sigma_3 = -\frac{Z+\sqrt{\Delta}}{2C^cC^s}, \tag{73}$$

$$\sigma_4 = -\frac{Z-\sqrt{\Delta}}{2C^cC^s}, \tag{74}$$

with

$$
\begin{aligned}
Z &= K(C^c + C^s) - C^s\kappa^c - C^c\kappa^s, && (75)\\
\Delta &= -4C^cC^s\left(\kappa^c\kappa^s - K\left(\kappa^c + \kappa^s\right)\right) + Z^2, && (76)\\
K &= \frac{3\beta^o}{n_6}\left(C^c - A^c + C^o_b - A^o_b\right), && (77)\\
\kappa^s &= \frac{3n_6}{2}\left(C^s - A^s + C^o_t - A^o_t\right), && (78)\\
\kappa^c &= \frac{3n_6}{2}\left(C^c - A^c + C^o_b - A^o_b\right). && (79)
\end{aligned}
$$

The periods associated, i.e. $T_3 = 2\pi/\sigma_3$ and $T_4 = 2\pi/\sigma_4$, are respectively between 200 and 260 years, and between 10 and 55 years. The range 200-260 years does not correspond to any obvious forcing, while the annual forcing, 29.46-yr periodic, can resonate with σ_4. Figure 7 shows the mean obliquity vs. T_4.

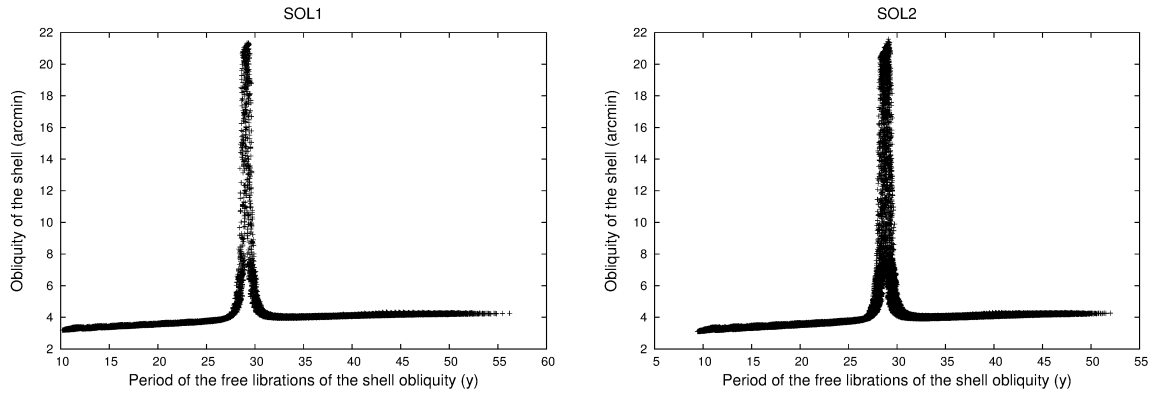

Fig. 7.— The resonance raising the obliquity of Titan. In the resonance, the averaging lacks reliability since the free oscillations are tricky to remove. The information to keep in mind is that in the resonance, the obliquity of the shell is likely to be much bigger than suggested by the secular behavior out of the resonance.

EDITOR: PLACE FIGURE 7 HERE.

The correlation between the obliquity and the resonance with the 29.46-yr periodic annual forcing is obvious. From the value of T_4, we estimate that 2,202 model Titans out of 20,546 for SOL1, i.e. 10.73%, are affected, and 6,540 out of 50,500 for SOL2, i.e. 12.95%, within the $3-\sigma$ limit. If we restrict to the $1-\sigma$ limit, then we have 234 model Titans over 2,237 for SOL1, i.e. 10.46%, and 354 over 2,665 for SOL2, i.e. 13.28%.

When a trajectory is resonant, getting rid of the free librations is very tricky and nearly impossible when working on a whole set of trajectories as we do in this Section. So, the numbers for the mean obliquity of the shell given in Fig.5 to 7 should not be considered as accurate in the resonant regime. The take-home message is that the resonance can raise the obliquity of these Titans to numbers bigger than the measured value. We will simulate some individual trajectories in Section 6.

5.3. Polar motion

We check the amplitude of the polar motion, often supposed to be small. Actually it is, the maximum amplitude being 3.5 km for the shell and 4.5 km for the core. Most of the trajectories have a polar motion much smaller than that.

6. Simulating the obliquity of the real Titan

The resonant obliquity of Titan's shell is highly sensitive to one frequency of the free oscillations of the obliquity, σ_4, itself dependent on the interior structure. For this reason, we propose here to build a synthetic representation of the obliquity of the shell with respect to the relevant frequency. This obliquity is given as a sum of a time series composed of trigonometric terms with numerical amplitudes. Using a synthetic theory to express the obliquity of a celestial body has already been done for Mercury (Noyelles & D'Hoedt 2012;

Noyelles & Lhotka 2013). Here the strategy is different since the periodic contributions involved, due to the orbital motion of Saturn about the Sun, have a much shorter period (≈ 30 years) than the relevant ones for Mercury, due to the regressional motion of Mercury's ascending node, the associated period being ≈ 250 kyears.

6.1. A synthetic model

Our goal is to express the obliquity of the shell as a sum:

$$K^s(t) = A_0 + \sum_i A_i \cos \phi_i(t), \tag{80}$$

where A_i are real amplitudes, and $\phi_i(t)$ linear functions of degree one of time. For that, we consider 13 models of Titan (see Tab.4) that fall into the resonance and correspond to the gravity solution SOL1 within the 1-sigma limit. Here the key parameter is the frequency σ_4 and the models have been chosen among this criterion, so choosing them in SOL2 instead of SOL1 would not change the results.

EDITOR: PLACE TABLE 4 HERE.

Table 4: Internal structure of the 13 resonant Titans that we use in this Section, complying with the SOL1 gravity field. The densities are in kg/m^3, the radii in km, and f is the compensation factor. 2440 km have been substracted from the radii of the shell-ocean boundary a_o, b_o and c_o, and 2170 km have been substracted from the radii of the core-ocean boundary a_c, b_c and c_c. The outer radii are the measured ones (Tab.1). All models had 130 km mean shell thicknesses, and all except N=58 had 270 km mean ocean thicknesses. The mean ocean thickness of the model 58 was 260 km.

N	ρ_s	ρ_o	ρ_c	a_o	b_o	c_o	a_c	b_c	c_c	f	J_2	C_{22}	Shell thickness
											$\times 10^{-5}$	$\times 10^{-6}$	Min - Max
58	900	950	2486.396	2.282	3.517	8.587	14.983	14.731	14.648	80%	3.147	9.973	125.843-132.868
791	910	960	2501.093	2.303	3.538	8.544	4.981	4.732	4.649	82%	3.176	9.949	125.885-132.847
1228	920	950	2502.910	0.469	2.733	11.184	4.980	4.732	4.649	82.5%	3.183	9.951	123.246-134.681
1230	920	950	2502.910	0.523	2.757	11.105	4.980	4.732	4.649	83.5%	3.207	9.966	123.325-134.627
1231	920	950	2502.910	0.550	2.768	11.067	4.980	4.732	4.649	84%	3.219	9.974	123.363-134.600
1333	920	960	2498.704	1.574	3.211	9.600	4.981	4.731	4.648	81.5%	3.168	9.961	124.830-133.576
1336	920	960	2498.704	1.636	3.239	9.511	4.981	4.731	4.648	83%	3.204	9.984	124.919-133.514
1485	920	980	2490.291	2.692	3.695	7.998	4.981	4.731	4.648	80%	3.148	9.988	126.432-132.457
1487	920	980	2490.291	2.721	3.708	7.956	4.981	4.731	4.648	81%	3.173	10.004	126.474-132.429
1488	920	980	2490.291	2.735	3.714	7.936	4.981	4.731	4.648	81.5%	3.186	10.012	126.494-132.415
1783	930	960	2496.315	0.442	2.705	11.239	4.981	4.731	4.648	82.5%	3.197	9.996	123.191-134.708
1858	930	970	2492.109	1.554	3.190	9.642	4.981	4.731	4.648	81.5%	3.181	10.005	124.788-133.596
1860	930	970	2492.109	1.596	3.209	9.581	4.981	4.731	4.648	82.5%	3.206	10.021	124.849-133.554

For each of these 13 models, we simulate the rotation corresponding to the dynamical equilibrium. For that, we use the algorithm of (Noyelles et al. 2014) already mentionned, consisting in removing iteratively the free oscillations from the initial conditions, after frequency analysis. The difficulty here comes from the quasi-resonant condition, because the period associated with σ_4 is close to the period of the annual forcing, i.e. 29.45716 years. To bypass this problem, we must integrate over a large time interval so that the distance between the frequencies gets bigger than twice the frequency whose period is the integration interval. In practice, we have integrated over 36,800 years. The TASS1.6 ephemeris are valid over 9,000 years, but since they are composed of trigonometric series, they can be extrapolated without diverging.

After obtaining the trajectories and frequency analysis of the obliquities, we get:

$$K^s(t,\sigma_4) \approx A_0(\sigma_4) + A_1(\sigma_4)\cos\phi_1(t) + A_2(\sigma_4)\cos\phi_2(t), \tag{81}$$

with

$$\phi_1(t) = 0.20436788\,t - 1.08611, \tag{82}$$

$$\phi_2(t) = 0.63989736\,t + 1.22080, \tag{83}$$

the time origin being J2000, the time in years, and the angles in radians. The periods of these forced oscillations are respectively 30.74475 and 9.81906 years. ϕ_1 and ϕ_2 can be reconstructed from the elements of Tab.3, numbered from (1) to (4). We have $\phi_1 = (1)-(4)$, and $\phi_2 = (3)-(4)$.

Tab.5 gathers the coefficients A_i given by the frequency analysis. The error due to this representation is always smaller than 1.1 arcmin over 100 years. This is actually a maximum of the difference between the obliquity given by the formula (81) and the one resulting from

our numerical simulation. This difference can be due to neglected oscillating contributions in the Eq.(81), but also to a residual of free oscillation in the numerical simulation, that noises the signal.

EDITOR: PLACE TABLE 5 HERE.

Table 5: Synthetic representation of the obliquity of the shell. The error due to the synthetic representation is estimated over 100 years from J2000. T_4 is the period associated with σ_4 measured by frequency analysis, while $T_4^\star$ is given by the Eq.(74). The last column gives the computed obliquity at the observation date, i.e. ≈2007.2. In this table, the models 58 and 1487 are the closest to the measured obliquity.

N	A_0 (arcmin)	A_1 (arcmin)	A_2 (arcmin)	Error (arcmin)	T_4 (years)	$T_4^\star$ (years)	ΔT_4	@J2007.2 (arcmin)
58	18.46293	−3.79374	0.58755	0.6	29.59253	29.25391	1.14%	15.4751
791	11.12233	3.70234	−0.57339	0.8	29.23168	28.75465	1.63%	14.0382
1228	9.10463	−3.67034	0.56454	0.9	29.74431	29.26631	1.61%	6.2105
1230	42.51503	3.75107	−0.59207	0.3	29.40183	28.85206	1.87%	45.4592
1231	11.05850	3.68666	−0.57384	0.8	29.23102	28.65278	1.98%	13.9594
1333	9.48745	−3.68069	0.56667	1.1	29.73195	29.30645	1.43%	6.5856
1336	10.17817	3.67598	−0.56950	0.8	29.20998	28.68037	1.81%	13.0731
1485	15.61029	−3.74199	0.58342	1.0	29.61870	29.26416	1.20%	12.6667
1487	12.79944	3.71361	−0.57774	0.7	29.26101	28.83270	1.46%	15.7218
1488	7.10257	3.58116	−0.53779	0.8	29.08751	28.62520	1.59%	9.9381
1783	9.48544	−3.66939	0.56698	1.1	29.73153	29.25060	1.62%	6.5944
1858	9.77734	−3.67887	0.56840	0.9	29.72422	29.29491	1.44%	6.8788
1860	29.96008	3.73986	−0.59003	0.4	29.37617	28.87354	1.70%	32.8957

We also check in this table the accuracy of the analytical estimation of T_4 by the Eq.(74). We can see that this formula slightly underestimates the period. Its accuracy, better than 2%, is good enough to detect the influence of the resonance, but might be insufficient to predict the resulting obliquity, since this quantity is highly sensitive to the distance to the exact resonance with the annual forcing. The last column gives $K^s(t = J2007.2)$ calculated from the Eq.(81), this date is very close to the one of the observation, i.e. March 11^{th}, 2007.

A least-square fit of the obtained numbers for A_0, A_1 and A_2 allows us to write

$$A_0 = \frac{\alpha}{|\sigma_4 - \sigma|}, \tag{84}$$

$$A_1 = \beta \,\mathrm{sgn}(\sigma_4 - \sigma), \tag{85}$$

$$A_2 = \gamma \,\mathrm{sgn}(\sigma - \sigma_4), \tag{86}$$

with

$$\alpha = (0.0176084 \pm 0.0002901)\,\mathrm{arcmin}, \tag{87}$$

$$\beta = (3.69780 \pm 0.01442)\,\mathrm{arcmin}, \tag{88}$$

$$\gamma = (0.573225 \pm 0.003937)\,\mathrm{arcmin}, \tag{89}$$

$\sigma = 2\pi/29.45716 = 0.2132991\, rad/y$ being the frequency of the annual forcing.

EDITOR: PLACE FIGURE 6 HERE.

The quantity A_0 can be seen as the mean obliquity of Titan, or of its shell, averaged over a long enough interval, here nearly 40 kyears. It should not be confused with the

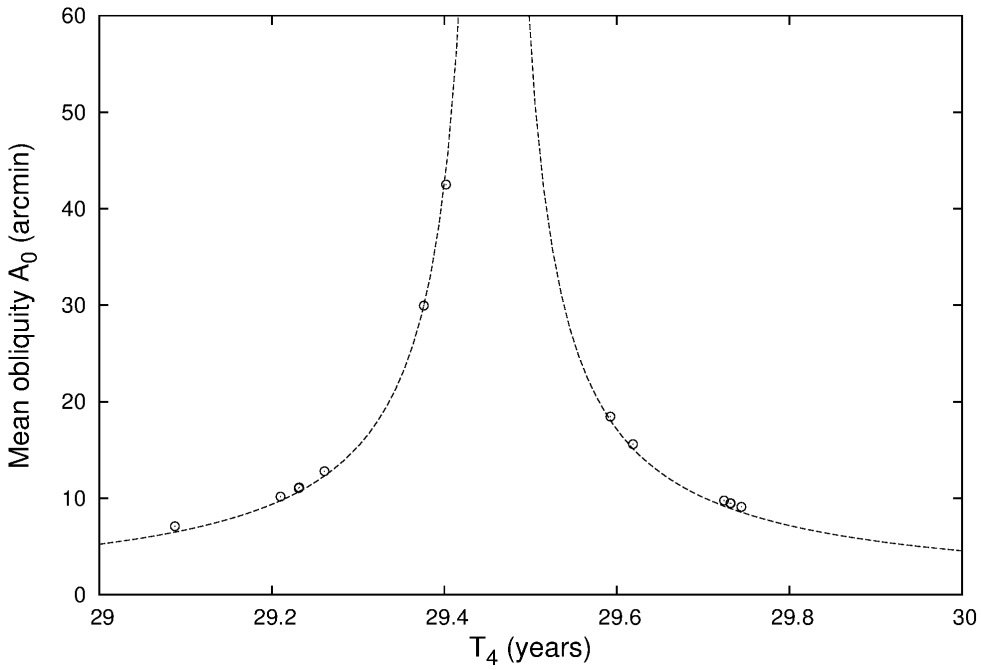

Table 6: Mean obliquity A_0 of Titan, fitted with the Eq.(84). The circles correspond to the models given in the Tab.5.

observed obliquity that is an instantaneous quantity. A_0 is plotted in the Fig.6. We can see an asymptotic behavior at the exact resonance, i.e. $\sigma_4 = \sigma$, or $T_4 = 29.45716$ years. The other two parameters A_1 and A_2 have a different sign whether σ_4 is bigger or smaller than σ.

6.2. 2 solutions

From the Eq.(81) we calculate the obliquity at J2007.2, to be compared to the (18.6 ± 3) arcmin measured by (Meriggiola & Iess 2012). We use our Eq.(81) instead of our numerical simulations, to remove the error due to the free oscillations. We get from a linear least squares fit:

$$K^s(t = J2007.2, \sigma_4) = \frac{\alpha'}{\|\sigma_4 - \sigma\|} + \beta' \,\mathrm{sgn}(\sigma - \sigma_4), \tag{90}$$

with

$$\alpha' = (0.0176424 \pm 0.0001689)\,\mathrm{arcmin}, \tag{91}$$

$$\beta' = (-2.73983 \pm 0.1727)\,\mathrm{arcmin}. \tag{92}$$

The Eq.(90) is plotted in the Fig.7.

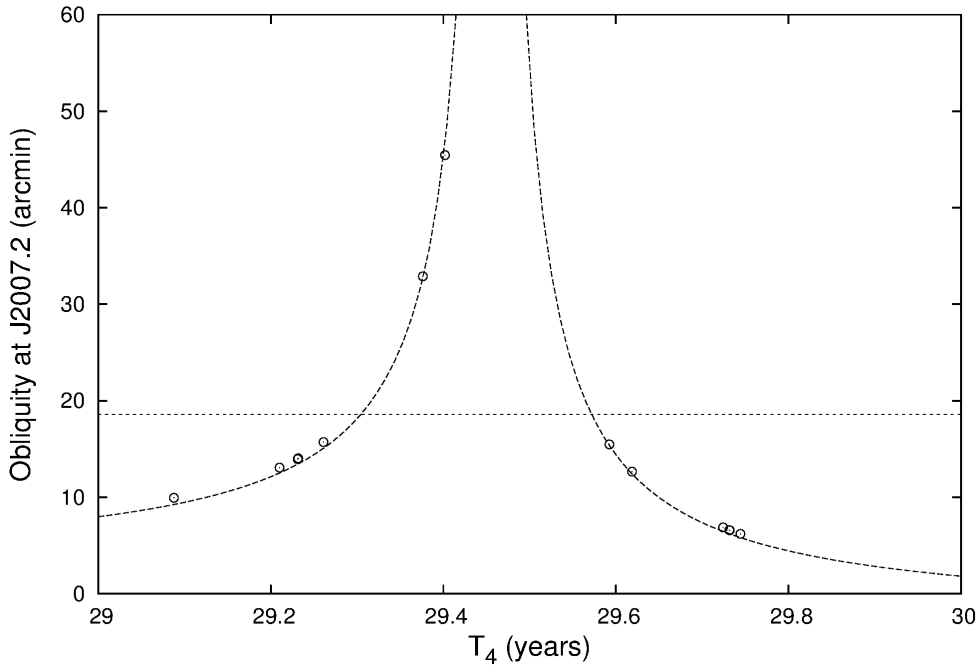

Table 7: Obliquity of Titan on March 11^{th}, 2007. The circles correspond to our 13 models, the associated obliquity being calculated with the Eq.(81). The plotted function is the Eq.(90), while the horizontal line corresponds to the 18.6 arcmin measured by (Meriggiola & Iess 2012). We can see that the problem has 2 solutions.

We can see that 2 frequencies, or periods, can give the measured obliquity of

18.6 arcmin. So, we have what we could call *left solutions*, where $T_4 < 29.45716$ years, or $\sigma_4 > \sigma$, and *right solutions* where $T_4 > 29.45716$ years, i.e. $\sigma_4 < \sigma$.

For left solutions we have $T_4 = 29.3 \pm 0.03$ years, and for right solutions $T_4 = 29.572^{+0.019}_{-0.015}$ years. These solutions are displayed in the Fig.8 over 100 years and in the Fig.9 over the duration of the *Cassini* mission.

EDITOR: PLACE FIGURE 8 HERE.

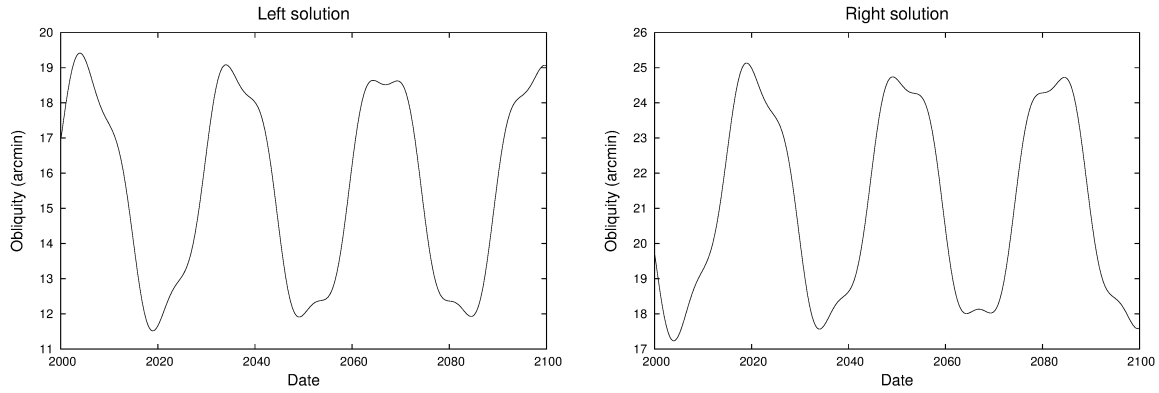

Fig. 8.— Left ($T_4 = 29.3$ years) and right ($T_4 = 29.572$ years) solutions over 100 years.

These two solutions coincide at the date of observation, but have actually very different behaviors. They have respectively a mean obliquity of ≈ 15 and ≈ 21 arcmin because the right solution is closer to the exact resonance than the left one, and they have the same period of main oscillation, i.e. 30.74475 years (Eq.82) but with opposite phases.

EDITOR: PLACE FIGURE 9 HERE.

As a consequence of these opposite phases, the left solution has a negative slope over the *Cassini* mission, while the right one has a positive one (see Tab. 8). A change in obliquity of roughly 7 arcmin (0.12°e) over the course of the *Cassini* mission is twice

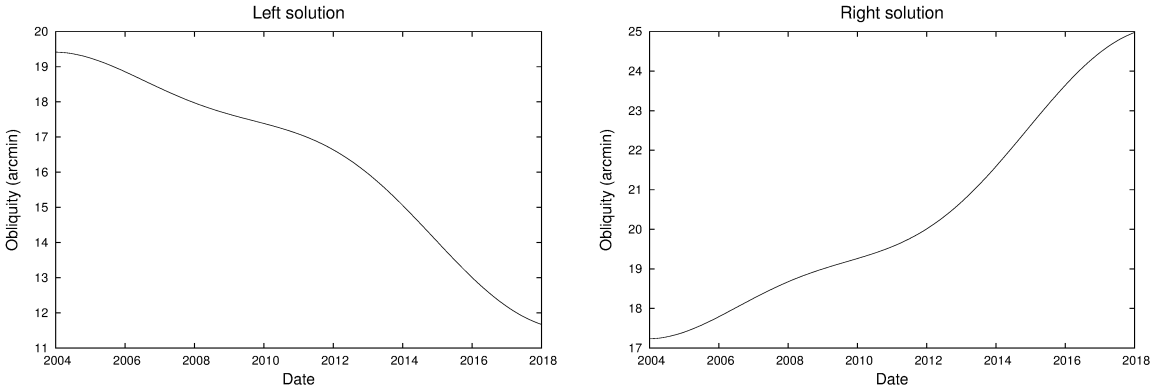

Fig. 9.— Left and right solutions over the *Cassini* mission.

the formal uncertainty quoted by Meriggiola & Iess (2012) and should be detectable with careful analysis (Bills et al. 2013).

EDITOR: PLACE TABLE 8 HERE.

Table 8: Mean slopes of the obliquity of Titan. The unit is arcsec/y.

	Left	Right
	$T_4 = 29.3$ y	$T_4 = 29.572$ y
$[2004; 2012]$	-20.8449	20.8449
$[2012; 2018]$	-49.6699	49.6699

6.3. The obliquity of the core

We also derived the mean obliquity of the core $< K^c >$, from a frequency analysis of the resulting trajectories. It is close to 9.2 arcmin, and the instantaneous core obliquity $K^c(t)$ can vary between 7 and 10.3 arcmin over the next 100 years. We also checked that the period T_3 of the free oscillations is slightly bigger than suggested by the analytical formula (73), the error being smaller than 1%.

7. Conclusion

The goal of this study was to investigate the constraint that the rotation of Titan could provide on its interior. Supporting the suggestion originally by (Baland et al. 2011), we find that between 10 and 13% of our realistic Titans fall into a resonance with the annual forcing, raising the obliquity of the shell. These Titans have a 130 to 140 km mean thickness shell overlying a ≈250 thick ocean, and include shell thickness variations (bottom loading) that are from 80% to 92% compensated, consistent with the gravity and topography constraints. A better determination of the gravity field would help to refine these numbers.

The quasi-resonant behavior results in two solutions to explain the observed obliquity of Titan, that could be discriminated by measuring the time derivative of the obliquity. A detection by *Cassini* of a time-variable obliquity would thus provide strong evidence for the analysis presented here.

Acknowledgments

Benoît Noyelles is an F.R.S.- FNRS postdoctoral research fellow. FN acknowledges support from the Cassini Participating Scientist Program.

A. Derivation of the gravitational torque of the shell on the crust

We here aim at deriving the gravitational torque of the shell on the crust as (Szeto & Xu 1997) did. We first express the vector $\vec{r}$ pointing to the position of a mass element of the core, in the reference frames of the shell and of the core:

$$\begin{aligned} \vec{r} &= X\vec{f_1^s} + Y\vec{f_2^s} + Z\vec{f_3^s} \\ &= x\vec{f_1^c} + y\vec{f_2^c} + z\vec{f_3^c} \end{aligned}$$

with

$$\begin{pmatrix} X \\ Y \\ Z \end{pmatrix} = \begin{pmatrix} l_1 & l_2 & l_3 \\ m_1 & m_2 & m_3 \\ n_1 & n_2 & n_3 \end{pmatrix} \begin{pmatrix} x \\ y \\ z \end{pmatrix} \tag{A1}$$

and

$$\begin{pmatrix} l_1 & l_2 & l_3 \\ m_1 & m_2 & m_3 \\ n_1 & n_2 & n_3 \end{pmatrix} = R_3(-\theta^s)R_1(-\epsilon^s)R_3(h^c - h^s)R_1(\epsilon^c)R_3(\theta^c), \tag{A2}$$

(X, Y, Z) and (x, y, z) being the cartesian coordinates of the mass element expressed in the two reference frames, of the shell and of the core respectively.

From

$$\begin{aligned} r^2 &= X^2+Y^2+Z^2, \\ \cos\psi &= Z/\sqrt{X^2+Y^2+Z^2}, \\ \sin^2\psi\cos 2\phi &= (X^2-Y^2)/(X^2+Y^2+Z^2), \\ P_2(\cos\psi) &= (2Z^2-X^2-Y^2)/(2(X^2+Y^2+Z^2)), \\ P_2^2(\cos\psi)\cos 2\phi &= 3(X^2-Y^2)/(X^2+Y^2+Z^2), \end{aligned}$$

we get

$$\Phi = \beta(2Z^2-X^2-Y^2)/2 + 3\gamma(X^2-Y^2). \tag{A3}$$

After expression of the potential Φ in the reference frame of the core following Eq.(A1), derivation to get the gradient and the cross product, and elimination of the crossed terms resulting in a null integral because the core is triaxial, we get from the Eq.(24):

$$\begin{aligned} \overrightarrow{\Gamma^c_{sh}} &= \beta \begin{bmatrix} (-2n_2n_3+m_2m_3+l_2l_3)\iiint_{core}\rho_c\,(z^2-y^2)\,dxdydz\overrightarrow{f_1^c} \\ (2n_1n_3-m_1m_3-l_1l_3)\iiint_{core}\rho_c\,(z^2-x^2)\,dxdydz\overrightarrow{f_2^c} \\ (-2n_1n_2+m_1m_2+l_1l_2)\iiint_{core}\rho_c\,(y^2-x^2)\,dxdydz\overrightarrow{f_3^c} \end{bmatrix} \\ &+ 6\gamma \begin{bmatrix} (m_2m_3-l_2l_3)\iiint_{core}\rho_c\,(z^2-y^2)\,dxdydz\overrightarrow{f_1^c} \\ (l_1l_3-m_1m_3)\iiint_{core}\rho_c\,(z^2-x^2)\,dxdydz\overrightarrow{f_2^c} \\ (m_1m_2-l_1l_2)\iiint_{core}\rho_c\,(y^2-x^2)\,dxdydz\overrightarrow{f_3^c} \end{bmatrix} \end{aligned} \tag{A4}$$

Since the matrix of the transformation from $\left(\overrightarrow{f_1^s},\overrightarrow{f_2^s},\overrightarrow{f_3^s}\right)$ to $\left(\overrightarrow{f_1^c},\overrightarrow{f_2^c},\overrightarrow{f_3^c}\right)$ is orthogonal as a product of orthogonal matrices, we have

$$\begin{aligned} l_1 l_2 + m_1 m_2 + n_1 n_2 &= 0, \\ l_1 l_3 + m_1 m_3 + n_1 n_3 &= 0, \\ l_2 l_3 + m_2 m_3 + n_2 n_3 &= 0. \end{aligned}$$

And from

$$\begin{aligned} \iiint\limits_{core} \rho_c \left(z^2 - y^2\right) dxdydz &= B^c - C^c, \\ \iiint\limits_{core} \rho_c \left(z^2 - x^2\right) dxdydz &= A^c - C^c, \\ \iiint\limits_{core} \rho_c \left(y^2 - x^2\right) dxdydz &= A^c - B^c, \end{aligned}$$

we finally obtain

$$\overrightarrow{\Gamma^c_{sh}} = 3\beta \begin{bmatrix} n_2 n_3 (C^c - B^c) \overrightarrow{f_1^c} \\ -n_1 n_3 (C^c - A^c) \overrightarrow{f_2^c} \\ n_1 n_2 (B^c - A^c) \overrightarrow{f_3^c} \end{bmatrix} + 6\gamma \begin{bmatrix} (l_2 l_3 - m_2 m_3)(C^c - B^c) \overrightarrow{f_1^c} \\ -(l_1 l_3 - m_1 m_3)(C^c - A^c) \overrightarrow{f_2^c} \\ (l_1 l_2 - m_1 m_2)(B^c - A^c) \overrightarrow{f_3^c} \end{bmatrix}, \quad \text{(A5)}$$

this formula being consistent with the Eq.7 of (Szeto & Xu 1997).

B. The NAFF algorithm

The frequency analysis algorithm that we use is based on Laskar's original idea, named NAFF as Numerical Analysis of the Fundamental Frequencies (see for instance (Laskar 1993) for the method, and (Laskar 2005) for the convergence proofs). It aims at identifying the coefficients a_k and ω_k of a complex signal $f(t)$ obtained numerically over a finite time span $[-T; T]$ and verifying

$$f(t) \approx \sum_{k=1}^{n} a_k \exp(\imath\omega_k t), \tag{B1}$$

where ω_k are real frequencies and a_k complex coefficients. If the signal $f(t)$ is real, its frequency spectrum is symmetric and the complex amplitudes associated with the frequencies ω_k and $-\omega_k$ are complex conjugates. The frequencies and amplitudes associated are found with an iterative scheme. To determine the first frequency ω_1, one searches for the maximum of the amplitude of

$$\phi(\omega) =< f(t), \exp(\imath\omega t) >, \tag{B2}$$

where the scalar product $< f(t), g(t) >$ is defined by

$$< f(t), g(t) >= \frac{1}{2T} \int_{-T}^{T} f(t) g(t)^* \chi(t) dt, \tag{B3}$$

$g(t)^*$ being the complex conjugate of $g(t)$. $\chi(t)$ is a weight function alike a Hann or a Hamming window, i.e. a positive function verifying

$$\frac{1}{2T} \int_{-T}^{T} \chi(t) dt = 1. \tag{B4}$$

Using such a window can help the determination in reducing the amplitude of secondary minima in the transform (B3). Its use is optional.

Once the first periodic term $\exp(\imath\omega_1 t)$ is found, its complex amplitude a_1 is obtained by orthogonal projection, and the process is started again on the remainder $f_1(t) = f(t) - a_1 \exp(\imath\omega_1 t)$. The algorithm stops when two detected frequencies are too close to each other, what alters their determinations, or when the number of detected terms reaches a limit set by the user. This algorithm is very efficient, except when two frequencies are too close to each other. In that case, the algorithm is not confident in its

accuracy and stops. When the difference between two frequencies is larger than twice the frequency associated with the length of the total time interval, the determination of each fundamental frequency is not perturbed by the other ones. Although the iterative method suggested by (Champenois 1998) allows to reduce this distance, some troubles may remain. In our specific case, the Titans affected by the annual resonance present a frequency of free oscillations that is very close to the forcing frequency of the Sun, the period associated being 29.46 years. For these Titans, distinguishing these two oscillations is challenging.

C. Analytical expression of the longitudinal librations

This calculation is not original and can be found for instance in (Baland & Van Hoolst 2010). We here write it in a way pretty similar as in (Van Hoolst et al. 2013). Our physical model is different because we do not consider elastic effects.

Since we are here only interested in the longitudinal librations, we can a priori assume that the obliquities and polar motions of the core and the shell are negligible. This yields $\omega_1^c = \omega_2^c = \omega_1^s = \omega_2^s = 0$ and $\epsilon^c = \epsilon^s = 0$, i.e. $\xi^c = \eta^c = \xi^s = \eta^s = 0$. So, only the Eq. 37, 40, 43 and 46 still hold. After expansion of the orbital ephemerides up to the first order in eccentricity e_6 and expression of the resonant arguments $\gamma^c = p^c - \lambda_6$ and $\gamma^s = p^s - \lambda_6$, we get:

$$C^s\ddot{\gamma^s} + K_1\gamma^s + K_2\gamma^c = 4eK_3 \sin \mathcal{M}_6, \tag{C1}$$

$$C^c\ddot{\gamma^c} + K_2\gamma^s + K_4\gamma^c = 4eK_5 \sin \mathcal{M}_6, \tag{C2}$$

with

$$K_1 = 3n_6^2\left(B^s - A^s + B_t^o - A_t^o\right) + 12\gamma^o\left(B^c - A^c + B_b^o - A_b^o\right), \quad \text{(C3)}$$

$$K_2 = -12\gamma^o\left(B^c - A^c + B_b^o - A_b^o\right), \quad \text{(C4)}$$

$$K_3 = \frac{3}{2}n_6^2\left(B^s - A^s + B_t^o - A_t^o\right), \quad \text{(C5)}$$

$$K_4 = \left(3n_6^2 + 12\gamma^o\right)\left(B^c - A^c + B_b^o - A_b^o\right), \quad \text{(C6)}$$

$$K_5 = \frac{3}{2}n_6^2\left(B^c - A^c + B_b^o - A_b^o\right), \quad \text{(C7)}$$

$\mathcal{M}_6$ being the mean anomaly of Titan. The amplitudes of the forced librations at orbital period g^s and g^c can be written as

$$g^s = \frac{4e\left(n_6^2 K_3 C^c + K_2 K_5 - K_3 K_4\right)}{C^c C^s\left(n_6^2 - \sigma_1^2\right)\left(n_6^2 - \sigma_2^2\right)}, \quad \text{(C8)}$$

$$g^c = \frac{4e\left(n_6^2 K_5 C^s + K_2 K_3 - K_1 K_5\right)}{C^c C^s\left(n_6^2 - \sigma_1^2\right)\left(n_6^2 - \sigma_2^2\right)}, \quad \text{(C9)}$$

where σ_1 and σ_2 are the frequencies of the free longitudinal oscillations:

$$\sigma_{1,2} = \frac{K_1 C^c + K_4 C^s \pm \sqrt{4(K_2^2 - K_1 K_4) C^c C^s + \left(K_1 C^c + K_4 C^s\right)^2}}{2C^c C^s}. \quad \text{(C10)}$$

D. Notations used in this paper

EDITOR: PLACE TABLE 9 HERE.

Table 9. Main notations used in this study.

a,b,c,R	External radii and mean radius of Titan
h^c,ϵ^c,θ^c	Euler angles orienting the principal axes of the core
h^s,ϵ^s,θ^s	Euler angles orienting the principal axes of the shell
ξ^c,η^c,p^c	Non-singular Euler coordinates for the core
ξ^s,η^s,p^s	Non-singular Euler coordinates for the shell
$\vec{G^c}$,$\vec{G^s}$	Angular momentum of the shell and the core
$(\vec{f_1^c}, \vec{f_2^c}, \vec{f_3^c})$	Reference frame of the principal axes of inertia of the core
$(\vec{f_1^s}, \vec{f_2^s}, \vec{f_3^s})$	Reference frame of the principal axes of inertia of the shell
A^c,B^c,C^c,A^s,B^s,C^s	Principal moments of inertia of the core and the shell
A_t^o,B_t^o,C_t^o,A_b^o,B_b^o,C_b^o	Principal moments of inertia of the top and bottom oceans
$\vec{r_{\text{ħ}}^s} = x_{\text{ħ}}^c \vec{f_1^c} + y_{\text{ħ}}^c \vec{f_2^c} + z_{\text{ħ}}^c \vec{f_3^c}$	Vector Titan-Saturn in the frame of the core
$\vec{r_{\text{ħ}}^s} = x_{\text{ħ}}^s \vec{f_1^s} + y_{\text{ħ}}^s \vec{f_2^s} + z_{\text{ħ}}^s \vec{f_3^s}$	Vector Titan-Saturn in the frame of the shell
$M_{\text{ħ}}$,M_6	Masses of Saturn and of Titan
n_6,$\mathcal{M}_6$,λ_6	Mean motion, anomaly and longitude of Titan
e_6,I_6	Eccentricity and inclination of Titan
ϖ_6,$\wp_6$	Longitudes of the pericentre and the ascending node of Titan
ρ_s,ρ_o,ρ_c,ρ_6	Densities of the shell, the ocean, the core, and Titan
a_o,b_o,c_o,a_c,b_c,c_c	Radii of the shell-ocean boundary and of the core
f_1,κ_1	Flattening and equatorial ellipticity of the shell-ocean boundary
f_2,κ_2	Flattening and equatorial ellipticity of Titan
ψ,ϕ	Colatitude and east longitude of a mass element
$\mathcal{G}$	Gravitational constant
$\vec{\Gamma_{\text{ħ}}^{s,o}}$	Gravitational torque of Saturn on the shell+top ocean
$\vec{\Gamma_{\text{ħ}}^{c,o}}$	Gravitational torque of Saturn on the core+bottom ocean

Table 9—Continued

$\overrightarrow{\Gamma_{co}^{s,o}}$	Gravitational torque of the core on the shell+top ocean
$\overrightarrow{\Gamma_{sh}^{c,o}}$	Gravitational torque of the shell on the core+bottom ocean
ψ^c,ψ^s	Tidal librations of the core and the shell
γ^c,γ^s	Physical librations of the core and the shell
g^c,g^s	Amplitude of the diurnal component of the physical librations
K^c,K^s	Obliquities of the core and the shell
Q_1^c,Q_2^c,Q_1^s,Q_2^s	Components of the polar motions of the core and the shell
d_o,d_s	Mean thicknesses of the shell and the ocean
h_t,h_b	Topographic top and bottom anomalies
f	Isostatic compensation factor
σ_1,σ_2,T_1,T_2	Frequencies and periods of the free librations in longitude
σ_3,σ_4,T_3,T_4	Frequencies and periods of the free librations of the obliquity

REFERENCES

Baland R.-M. & Van Hoolst T., 2010, Librations of the Galilean satellites: The influence of global internal liquid layers, Icarus, 209, 651-664

Baland R.-M., Van Hoolst T., Yseboodt M. & Karatekin Ö., 2011, Titan's obliquity as evidence of a subsurface ocean?, A&A, 530, A141

Bills B.G. & Nimmo F., 2008, Forced obliquity and moments of inertia of Titan, Icarus, 196, 293-297

Bills B.G. & Nimmo F., 2011, Rotational dynamics and internal structure of Titan, Icarus, 214, 351-355

Bills B.G., Stiles B., Kirk R., Howington-Kraus E., Redding B., Lee E. & Merigiolla R, 2013, Titan rotation: constraints from Cassini radar, Lunar Planet. Sci. Conf., 44, 1313

Black G.J., Nicholson P.D. & Thomas P.C., 1995, Hyperion: rotational dynamics, Icarus, 117, 149-161

Bois E. & Rambaux N., 2007, On the oscillations in Mercury's obliquity, Icarus, 192, 308-317

Cassini G.D., 1693, Traité de l'origine et du progrès de l'astronomie, Paris

Cebron D., Le Bars M., Moutou C. & Le Gal P., 2012, Elliptical instability in terrestrial planets and moons, A&A, 539, A78

Champenois S., 1998, Dynamique de la résonance entre Mimas et Téthys, premier et troisième satellites de Saturne, Ph.D. Thesis, Observatoire de Paris, in French

Choukroun M. & Sotin C., 2012, Is Titan's shape caused by its meteorology and carbon cycle?, Geophys. Res. Lett., 39, L04201

Colombo G., 1966, Cassini's Second and Third Laws, AJ, 71, 891-896

Couetdic J., Laskar J., Correia A.C.M., Mayor M. & Udry S., 2010, Dynamical stability analysis of the HD202206 system and constraints to the planetary orbits, A&A, 519, A10

Delsate N., 2011, Analytical and numerical study of the ground-track resonances of Dawn orbiting Vesta, Planet. Space Sci., 59, 1372-1383

Dufey J., Noyelles B., Rambaux N. & Lemaître A., 2009, Latitudinal librations of Mercury with a fluid core, Icarus, 203, 1-12

Fortes A.D., Grindrod P.M., Trickett S.K. & Vocadlo L., 2007, Ammonium sulfate on Titan: Possible origin and role in cryovolcanism, Icarus, 188, 139-153

Fortes A.D., 2012, Titan's internal structure and the evolutionary consequences, Planet. Space Sci., 60, 10-17

Fowles G.R. & Cassiday G.L., Analytical Mechanics: Sixth Edition, Thomson Learning Inc., Wadsworth

Goldreich P.M. & Mitchell J.L., 2010, Elastic ice shells of synchronous moons: Implications for cracks on Europa and non-synchronous rotation of Titan, Icarus, 209, 631-638

Grasset O. & Sotin C., 1996, The cooling rate of a liquid shell in Titan's interior, Icarus, 123, 101-112

Grasset O., Sotin C. & Deschamps F., 2000, On the internal structure and dynamics of Titan, Planet. Space Sci., 48, 617-636

Hairer E., Nørsett S.P. & Wanner G., 1993, Solving Ordinary Differential Equations I, Springer, Berlin

Harbison R.A., Thomas P.C. & Nicholson P.C., 2011, Rotational modeling of Hyperion, Celestial Mechanics and Dynamical Astronomy, 110, 1-16

Hemingway D., Nimmo F., Zebker H. & Iess L., 2013, A rigid and weathered ice shell on Titan, Nature, 500, 550-552

Iess L., Rappaport N.J., Jacobson R.A., Racioppa P., Stevenson D.J., Tortora P., Armstrong J.W. & Asmar S.W., 2010, Gravity field, shape, and moment of inertia of Titan, Science, 327, 1367-1369

Iess L., Jacobson R.A., Ducci M., Stevenson D.J., Lunine J.I., Armstrong J.W., Asmar S.W., Racioppa P., Rappaport N.J. & Tortora P., 2012, The tides of Titan, Science, 337, 457-459

Jara-Orué H.M. & Vermeersen B.L.A., 2014, The forced libration of Europa's deformable shell and its dependence on interior parameters, Icarus, 229, 31-44

Jeffreys H., 1952, The Earth: Its origin, history and physical constitution, Cambridge University Press, Cambridge

Laskar J., 1993, Frequency analysis of a dynamical system, Celestial Mechanics and Dynamical Astronomy, 56, 191-196

Laskar J., 2005, Frequency map analysis and quasiperiodic decomposition, in Hamiltonian systems and Fourier analysis: new prospects for gravitational dynamics, in: Benest et al. (ed.), Cambridge Sci. Publ., 99-129

Lebonnois S., Burgalat J., Rannou P. & Charnay B., 2012, Titan global climate model: A new 3-dimensional version of the IPSL Titan GCM, Icarus, 218, 707-722

Lunine J.I. & Stevenson D.J., 1987, Clathrate and ammonia hydrates at high pressure: Application to the origin of methane on Titan, Icarus, 70, 61-77

MacMillan W.D., 1936, Dynamics of Rigid Bodies, McGraw-Hill, New York

Meriggiola R. & Iess L., 2012, A new rotational model of Titan from Cassini SAR data, European Planetary Science Congress 2012, id. EPSC2012-593

Murray C.D. & Dermott S.F., 2000. Solar System Dynamics. Cambridge University Press, Cambridge

Nimmo F. & Bills B.G., 2010, Shell thickness variations and the long-wavelength topography of Titan, Icarus, 208, 896-904

Noir J., Hemmerlin F., Wicht J., Baca S.M. & Aurnou J.M., 2009, An experimental and numerical study of librationally driven flow in planetary cores and subsurface oceans, Physics of the Earth and Planetary Interiors, 173, 141-152

Noyelles B., Lemaitre A. & Vienne A., 2008, Titan's rotation: A 3-dimensional theory, A&A, 478, 959-970

Noyelles B., 2008, Titan's rotational state: The effects of a forced "free" resonant wobble, Celestial Mechanics and Dynamical Astronomy, 101, 13-30

Noyelles B., 2009, Expression of Cassini's third law for Callisto, and theory of its rotation, Icarus, 202, 225-239

Noyelles B., 2010, Theory of the rotation of Janus and Epimetheus, Icarus, 207, 887-902

Noyelles B., Karatekin Ö. & Rambaux N., 2011, The rotation of Mimas, A&A, 536, A61

Noyelles B. & D'Hoedt S., 2012, Modeling the obliquity of Mercury, Planet. Space Sci., 60, 274-286

Noyelles B. & Lhotka C., 2013, The influence of orbital dynamics, shape and tides on the obliquity of Mercury, Advances in Space Research, 52, 2085-2101

Noyelles B., Delsate N. & Carletti T., 2014, Equilibrium search algorithm of a perturbed quasi-integrable system, submitted

Peale S.J., 1969, Generalized Cassini's Laws, AJ, 74, 483-489

Peale S.J., Yseboodt M. & Margot J.-L., 2007, Long-period forcing of Mercury's libration in longitude, Icarus, 187, 365-373

Ramsey A.S., 1937, Dynamics – Part 2, Cambridge University Press, Cambridge

Ramsey A.S, 1940, An introduction to the theory of Newtonian attraction, Cambridge University Press, Cambridge

Richard A., Rambaux N. & Charnay B., 2014, Librational response of a deformed 3-layer Titan perturbed by non-keplerian orbit and atmospheric couplings, Planet. Space Sci., in press, http://dx.doi.org/10.1016/j.pss.2014.02.006

Robutel P., Rambaux N. & Castillo-Rogez J., 2011, Analytical description of physical librations of saturnian coorbital satellites Janus and Epimetheus, Icarus, 211, 758-769

Sohl F., Hussmann H., Schwentker B., Spohn T. & Lorenz R.D., 2003, Interior structure models and tidal Love numbers of Titan, J. Geophys. Res., 108, E12, 5130

Sotin C., Mitri G., Rappaport N., Schubert G. & Stevenson D., 2010, Chapter 4: Titan's interior structure, in: Titan from Cassini-Huygens, Brown R.H., Lebreton J.-P. and Waite J.H. eds, Springer

Stiles B.W., Kirk R.L., Lorenz R.D., Hensley S., Lee E., Ostro S.J., Allison M.D., Callahan P.S., Gim Y., Iess L., Persi Del Marmo P., Hamilton G., Johnson W.T.K. & West

R.D., 2008, Determining Titan's spin state from CASSINI RADAR images, AJ, 135, 1669-1680

Szeto A.M.K. & Xu S., 1997, Gravitational coupling in a triaxial ellipsoidal Earth, J. Geophys. Res., 102, 27651-27657

Tobie G., Grasset O., Lunine J.I., Mocquet A. & Sotin C., 2005, Titan's internal structure inferred from a coupled thermal-orbital model, Icarus, 175, 496-502

Tokano T. & Neubauer F.M., 2005, Wind-induced seasonal angular momentum exchange at Titan's surface and its influence on Titan's length-of-day, Geophys. Res. Lett., 32, L24203-L24206

Tokano T., Van Hoolst T. & Karatekin Ö., 2011, Polar motion of Titan forced by the atmosphere, J. Geophys. Res., 116, E05002

Van Hoolst T., Rambaux N., Karatekin Ö., Dehant V. & Rivoldini A., 2008, The librations, shape, and icy shell of Europa, Icarus, 195, 386-399

Van Hoolst T., Rambaux N., Karatekin Ö. & Baland R.-M., 2009, The effect of gravitational and pressure torques on Titan's length-of-day variations, Icarus, 200, 256-264

Van Hoolst T., Baland R.-M. & Trinh A., 2013, On the librations and tides of large icy satellites, Icarus, 226, 299-315

Vienne A. & Duriez L., 1995, TASS1.6: Ephemerides of the major Saturnian satellites, A&A, 297, 588-605

Watts A.B., 2001, Isostasy and flexure of the lithosphere, Cambridge University Press, Cambridge

Williams J.G., Boggs D.H., Yoder C.F., Ratcliff J.T. & Dickey J.O., 2001, Lunar rotational dissipation in solid body and molten core, J. Geophys. Res., 106, 27933-27968

Yseboodt M. & Margot J.-L., 2006, Evolution of Mercury's obliquity, Icarus, 181, 327-337

Zebker H.A., Stiles B., Hensley S., Lorenz R., Kirk R.L. & Lunine J., 2009, Size and shape of Saturn's moon Titan, Science, 324, 921-923

This manuscript was prepared with the AAS LaTeX macros v5.2.

List of Tables

1 The shape of Titan. 3

2 The 2 solutions for the gravity field of Titan. 19

3 Orbital inclination and ascending node of Titan. 21

4 Internal structure of 13 resonant Titans. 42

5 Synthetic representation of the obliquity of Titan. 44

6 Mean obliquity of Titan. 46

7 Obliquity of Titan on March 11^{th}, 2007. 47

8 Mean predicted time-derivatives of the obliquity of Titan. 49

9 Main notations used in this study. 57

9 Main notations used in this study. 58

List of Figures

1 The Euler angles. 20

2 Properties of our Titans. 33

3 Thickness variations of the shell of our Titans. 34

4 Longitudinal librations of the shell. 35

5 Influence of the thickness of the shell on its obliquity. 37

6 Influence of the thickness of the ocean on the obliquity of the shell. 38

7 The resonance raising the obliquity of Titan. 39

8 Left ($T_4 = 29.3$ years) and right ($T_4 = 29.572$ years) solutions over 100 years. 48

9 Left and right solutions over the *Cassini* mission. 49